

A-mode Breast Imaging

An investigative study of characterization and verification of an ultrasound probe that comprises multiple A-mode transducers

S. Dellarosa

A-mode Breast Imaging

An investigative study of characterization and verification of an ultrasound probe that comprises multiple A-mode transducers

by

S. Dellarosa

to obtain the degree of Master of Science

at the Delft University of Technology,

to be defended publicly on Thursday, September 10, 2020 at 11:00 AM.

Student number: 4783344

Project duration: November 4, 2019 – September 10, 2020

Thesis committee: dr. ir. R. F. Remis, TU Delft, supervisor
A. van Genderen, TU Delft
A. Stanton, TOPIC Embedded Systems
D. van den Heuvel, TOPIC Embedded Systems

An electronic version of this thesis is available at <http://repository.tudelft.nl/>.

Preface

I would like to thank my supervisor from the TU Delft, Rob, for guiding me throughout the whole process, as well as my supervisors from TOPIC, Dirk and Annamarie for this opportunity and also for their guidance. I would like to thank my family for their continuous support and lastly, I would like to thank the TU Delft | Global Initiative, as without them I would not have been able to take part in this tremendous journey.

*S. Dellarosa
Delft, September 2020*

Abstract

Breast cancer, as one of the main causes of cancer death in the world, requires early detection to increase rate of survival. One idea is to develop a device that women could use at home to perform a regular self-check. Ultrasound is a safe, radiation-free technology that could be used for this device. Ultrasound systems (B-mode) that are typically used in a hospital however, are too expensive for the general population. The older ultrasound technology called A-mode, could be repurposed for this device as it costs a lot less. A-mode scans are seldom used at the present time, as B-mode scans have proven to be much more powerful for use in medical diagnostics. However, the costs of manufacturing a B-mode probe is a lot higher than an A-mode probe. This is especially important in the development of a portable ultrasound probe where costs are constrained. This study attempts to investigate how an ultrasound probe that comprises multiple A-mode transducers could be used together for breast cancer detection. Specifically, the aim of this study is to characterize and verify an ultrasound probe that comprises multiple A-mode transducers. To this end, a simulation environment is developed in MATLAB using the k-Wave toolbox, where an ultrasound probe is described through a set of input parameters and outputs its response when placed on the skin of breast tissue. The breast phantom models are generated from software in the Virtual Imaging Clinical Trial for Regulatory Evaluation (VICTRE) trial and have four different levels of density as defined in BI-RADS. Two masses, one of benign and the other malignant nature were examined. The input parameters distance between the transducers, input frequency, and number of transducers, are investigated by comparing their responses in terms of contrast ratio around a breast mass. Towards the end, comparison to B-mode imaging are also made. Based on the results, the distance between transducers yields better performance with a higher value, as long as it does not go beyond the size of the mass. Higher input frequency also contributed to a better contrast ratio value. The number of transducers did not seem to have a correlation to the performance, with respect to contrast ratio values. However, when converted to a pseudo (very narrow) B-mode image, a higher number of transducers seem to very slightly mimic what might appear in a B-mode image. Upsampling it to account for the distance between the transducers, as well as to create a wider image seemed to improve the results.

Contents

1	Introduction	1
1.1	Breast Cancer	1
1.2	Research Scope	2
1.2.1	Objective.	2
1.2.2	Research Questions	3
1.3	Challenges	3
1.4	Approach	3
1.5	State of the Art	4
1.6	Thesis Outline	5
2	Theoretical Background	7
2.1	Ultrasound Imaging.	7
2.1.1	Physics of Ultrasound	7
2.1.2	Ultrasound Transducers	8
2.1.3	Beam Profile	8
2.1.4	Signal Processing	9
2.1.5	Acoustic Artifacts	10
2.1.6	Advanced Processing Methods.	11
2.2	Ultrasound for Breast Imaging	11
2.2.1	Characteristics of Breast Masses	12
2.2.2	Methods for Malignancy Detection	12
2.2.3	BI-RADS	13
2.3	Related Work	13
3	Methodology	15
3.1	Design	15
3.2	Numerical Models	15
3.2.1	Breast Phantom Models	17
3.2.2	Breast Mass Models	17
3.3	Acoustic Wave Propagation	18
3.4	Simulation Layout	19

3.5	Simulation Parameters	20
3.5.1	Input Parameters	20
3.5.2	Boundary Conditions	21
3.5.3	Signal Processing	22
3.6	Design Requirements	22
3.7	Computational Pipeline.	23
4	Experimental Results	25
4.1	Preliminary Runs	25
4.1.1	Basic Settings	25
4.1.2	Mass Variations	26
4.1.3	Density Variations	26
4.2	Distance Between Transducers	29
4.3	Input Frequency	29
4.4	Number of Transducers	32
4.5	Comparison with B-mode.	32
4.6	Transducer Size	34
4.7	Comparison with Real Data	35
5	Conclusion	37
A	Complementary Results	39
A.1	Various Input Frequencies	39
A.2	Various Transducer Distance	41
	Bibliography	43

Introduction

This chapter explains the context and motivation of the research. Section 1.1 provides the background and importance of research in the field of breast cancer. Section 1.2 defines the scope of the research and lists the research questions that this thesis study attempts to answer. In Section 1.3, the challenges that are faced during the study are briefly discussed. Section 1.4 describes the approach taken in tackling the research questions. Current state-of-the-art related to the research topic is explored in Section 1.5. Section 1.6 outlines the structure of the thesis report.

1.1. Breast Cancer

Breast cancer is one of the leading causes of cancer death in the world. In 2018, it is the second most commonly diagnosed of all new cancer cases in 185 countries [1]. Around 2.1 million people were diagnosed, accounting for almost 1 in 4 cancer cases among the female populations, and more than 600,000 of these cases were fatal. In the Netherlands, breast cancer is the most prevalent type of cancer diseases [1]. Early detection is therefore highly important as it has been shown to significantly increase cancer survival rate [2, 3]. When found early, where it still has a relatively small size and is still confined within the breast, there is a higher chance of treating the cancer successfully. The American Cancer Society recognizes this as the localized stage, in which the 5-year relative survival rate is estimated at around 99% [4].

Attempts to eliminate breast cancer operate in three parts: screening, diagnosis, and treatment. A breast cancer screening test is performed routinely in hopes of detecting the presence of breast cancer at an early stage, before any symptoms appear. A diagnostic test aims to determine whether a person suspected of having breast cancer actually does so. Once the person is confirmed to have breast cancer, the treatment process will commence and will be adapted according to the type of the cancer. A test will be performed regularly to check for the progress of the treatment.

Screening and diagnosis of breast cancer could be carried out by detecting the presence of a palpable mass within the breast tissues. There are many methods to perform such a detection. *Clinical Breast Exam* (CBE), or Breast Physical Exam, is a manual inspection of breast cancer performed carefully by a healthcare professional who is trained to identify many different types of abnormalities. *Mammography* uses X-rays to examine for breast pathology. To this day, mammography is still the most widely used breast screening procedure. Despite being considered as the most informative methods for breast cancer diagnosis [5], a main disadvantage of mammography, however, is that it involves the use of a dose of ionizing radiation, therefore causing a harmful exposure to the patient. *Magnetic Resonance Imaging* (MRI) utilizes strong magnetic field and a pulse of radio waves to construct a set of tomographic images of the breast. In *ultrasound* imaging, high frequency sound, or ultrasound, waves are emitted from a probe on the patient's breast skin. They travel through breast tissues until the density difference between the cancer mass and the surrounding tissues causes the ultrasound waves to be reflected and detected by the probe sensors.

The diagnostic values of each screening method can be expressed in terms of their sensitivity (true posi-

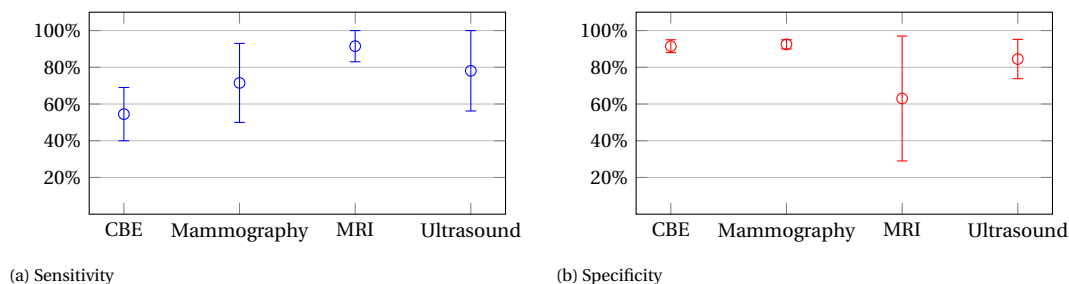


Figure 1.1: Comparison of diagnostic values of different breast screening methods

tive rate) and specificity (true negative rate). The values are obtained from [5, 6] and are depicted in Figure 1.1. While MRI is seen to have a high sensitivity value, it also has a very wide range of specificity, from which it can be deduced that MRI is more prone to providing false positives more than the other screening methods. Mammography and ultrasound score relatively high in terms of both their sensitivity and specificity.

Ultrasound differs from mammography in that it is completely safe on account of the absence of exposure to radiation. It also exhibits an advantage by allowing for computerized processing, as the data provided is suitable for digitization. When compared to MRI, the technology of ultrasound is rather inexpensive.

1.2. Research Scope

The research scope of this thesis will be explained in two parts. First, the main objective that this thesis aims to achieve will be described, from which a list of research questions are derived.

1.2.1. Objective

With the importance of early detection, the idea arises that a breast screening method should be highly accessible. This means providing access as close to the patients as possible. In the grand scheme of things, the proposal is for the development of a handheld ultrasound probe for breast cancer screening that women could use from the comfort of their home. This thesis study aims to serve as the starting point of its development.

As accessibility would often translate to affordability, there is a cost constraint that must be considered in the production of such a device. While ultrasound imaging is considerably less expensive than other imaging methods such as MRI, this only applies within the context of hospital use. Current state-of-the-art ultrasound devices are still largely unaffordable for most of the population. B-mode ultrasound imaging is the technology that possesses the ability to produce an acoustic image in 2D, and with recent innovations in the field of ultrasound, also in 3D. The technology that precedes it is called A-mode ultrasound imaging, which is a purely one-dimensional scanning method in which the ultrasound probe only has a single-transducer element, whereas in B-mode imaging multiple elements are used in an array. Since the cost of manufacturing A-mode probes are much less than that of B-mode probes, it seems fitting to utilize A-mode imaging for the proposed device.

However, unlike B-mode imaging that could generate an acoustic image of scanned tissue, A-mode imaging only produces a 1D output that is the echo response of the transmitted ultrasound pulse, in function of time. Therefore, the novelty comes in making use of a number of single-element transducers concurrently in one probe, to create a pseudo B-mode imaging. The most important question to answer is how this combination of 1D output of the transducers may be used to gain useful information about the underlying structure of scanned tissue. In other words, to ultimately identify whether an abnormal mass exists within the breast, and whether it is of a cancerous or non-cancerous nature. While there are many design and architectural details that need to be taken under consideration, two of the main areas of focus would be optimization of the probe's design parameters such that the output generated contains the most valuable information and methods to use the output for identification and classification of an abnormal mass in the breast. This thesis focuses on the former. Hence, finally, the topic of this thesis study is defined as an investigative study of

characterization and verification of an ultrasound probe that comprises multiple A-mode transducers.

1.2.2. Research Questions

Several research questions are then derived are derived from the main research topic.

RQ1 Characterization: how do different design parameters affect the behavior of the probe?

- (a) What are the design parameters to be investigated?
- (b) How do the parameters affect one another as well as the output?
- (c) How can the behavior of the probe be modeled?

RQ2 Verification: How could we ensure that the design requirements have been met?

- (a) What are the design requirements of the ultrasound probe?
- (b) Which set of input parameters result in optimized outcomes?
- (c) What could be achieved by the system, in comparison to B-mode imaging?

1.3. Challenges

The invention of B-mode imaging has steered away the research field of ultrasound from its initial focus of A-mode imaging. The past decades have seen a huge increase in the number of studies of B-mode ultrasound and a quick decline of the A-mode. While it is difficult to overcome this challenge, an attempt was made by translating the methods studied in B-mode imaging in terms of A-mode imaging.

Due to the large number of factors involved, the development of an ultrasound probe is a highly challenging task. It is a multivariate problem that involves a great number of factors that not only affect the output result but also interact with each other in complex relationships. It is therefore important to focus only on certain aspects of the transducer. Only a certain set of parameters will have their values changed, while most of the other variables will have a constant value, such that the the effect of those parameters may be visible in the output.

One of the main reasons the medical field has shifted its focus towards B-mode imaging is the vast amount of information that a B-mode scanner is able to gather during a scan, which are then used to construct 2D, perhaps sometimes 3D, images of the underlying tissue structure. On the contrary, only lines of echoes are obtained while working with A-mode imaging. This may be a cause for difficulty in the analysis of the experimental results. Other than simply comparing the responses visually, certain metric, that extracts features from the echo lines, will need to be defined such that the results could be compared in quantitative terms.

1.4. Approach

The investigative study will be carried out in a systematic approach, based on a standard procedure for design of experiments, which allows for the study of both individual and interactive effects of multiple design factors that could affect the output results [7]. The steps that will be taken are summarized below.

1. Specification of input parameters, boundary conditions, output metrics. Input parameters are the parameters that are used in the design of the ultrasound probe that are being studied. Boundary conditions are the parameters that remain constant in all of the experiments. They are not the primary concern of the experimental outcome and are mostly environmental variables. The output metrics are the metrics that are being used to compare the output of the experiments.
2. Formulation of design requirements, which indicate the performance of the input parameters. These are the objectives that are to be evaluated for a specific set of input parameters. This is necessary, as for example, a certain parameter may results in an optimal output with breast of extreme density, but falls short with breast of lower density.

3. Preparation of the simulation model. This relates to the tools that are used to simulate the ultrasound propagation, the digital breast phantoms, as well as the acoustic parameters that define these phantoms.
4. Investigation of different parameters. As the last step, this concerns executing the experiments using different values for each input parameters, collecting the results, and discussing the observations to learn how a specific parameter affects the response obtained.

1.5. State of the Art

Attempts to make breast cancer imaging more accessible and affordable have been investigated in numerous studies. However, there has not been any that specifically discusses reusing A-mode imaging for breast cancer screening. Some of the studies also make use of technologies other than ultrasound to detect the presence of tumor, which is discussed in the following. Since A-mode has not recently been used for breast imaging, a recent albeit different use of A-mode ultrasound is also described.

Xu et al. [8] developed iBreastExam (iBE) for UE LifeSciences Inc., which is a handheld device that uses piezoelectric finger (PEF) detector for early detection of breast cancer. A PEF detector is essentially a tissue-stiffness sensor with two piezoelectric lead zirconate titanate (PZT) layers placed on the top and bottom part of stainless steel, which is able to measure the tissue stiffness (in vivo, under compression), called the elastic modulus. The top PZT layer is used to drive the PEF to bend when a voltage is applied, while the bottom PZT layer functions to sense displacements to provide an accurate measurement of the elastic modulus of the tissue. The technology has been described as “ideal for electronic palpation”, and like ultrasound, is radiation-free. It was concluded in the study that PEF is ideal for prescreening of breast tumor. Although, it is important to note that while PEF has shown to successfully identify presence of a breast tumor, is not able to differentiate the malignancy of the tumor. iBE, which uses PEF, has been validated in numerous clinical studies [9–11]. According to Haas [12], the machine itself costs USD 10 000, while each patient is only required to pay a very small amount, between USD 1–3, for each scan. iBE is used in clinics in 12 countries, most of which are low-resource, developing countries.

One particular study was designed to demonstrate that computer-assisted diagnosis may be used, in combination with a low-cost ultrasound probe, to determine breast tumor malignancy. Love et al. [13] conducted the study in low- to middle-income countries to show that this is an effective approach that can be operated even by healthcare workers with minimal training, which will eventually lead to an affordable imaging method for environments with scarce resources. The research did not construct its own novel hardware to perform the ultrasound scans, but rather it used a low-cost portable ultrasound device from General Electric, the GE Vscan Dual Probe (GE Vscan Dual Probe; General Electric Medical Systems, Waukesha, WI, United States). It is equipped with a 8-MHz linear array transducer (B-mode). While this can be categorized as low cost, relative to other available machines with similar functionalities, per GE’s website [14] this ultrasound probe is priced between USD 4 995–6 095, depending on the configuration.

With regards to A-mode imaging, it has recently been discussed as a method to measure body composition. Smith-Ryan et al. [15] investigated the validity and reliability of a portable ultrasound probe operating in A-mode for measurement of body composition. The study uses the low-cost BodyMetrix Professional BX-2000 ultrasound system (BodyMetrix, Intelametrix, Livermore, CA, United States), a 2.5-MHz A-mode probe that measures subcutaneous fat thickness, which to the knowledge of the authors, is the only available ultrasound device that is designed to measure body fat composition that uses the A-mode technology. On its official website [16], the device is listed for USD 2 495. The study found that A-mode ultrasound provides a respectable reliability in terms of the calculated percent body fat and fat mass, which were calculated using the 7-site Jackson and Pollock equation. Wagner et al. [17] compares the results of the measurement of the same device with those obtained using a much more expensive, 12-MHz ultrasound system. With the B-mode system, the body fat composition was calculated by manually dissecting the thicknesses from the B-mode images. The authors concluded that the two results were not significantly different.

As is already evident from above, “low-cost” ultrasound devices, while considerably less expensive than a standard B-mode ultrasound system used in hospitals, are still largely unaffordable for most of the population. If the objective of the study is to ultimately build an ultrasound device that women can use at home, a

lot of research needs to be conducted to ensure that the limited extent of technology that could be used given the cost constraint, is able to provide valid results. Nevertheless, it is encouraging to know that in certain applications, A-mode ultrasound has been demonstrated to yield respectable results, when compared to those achieved in B-mode.

1.6. Thesis Outline

Chapter 2 covers the theoretical knowledge necessary for the foundation of this thesis study. The topics include: the basic principles of ultrasound imaging, the use of ultrasound imaging as a modality for breast cancer screening, and literature related to the design of an ultrasound probe. Chapter 3 details the design process of the experiment and the tools necessary in building the simulation environment. Chapter 4 delivers the experimental results and provides discussions as well as an analysis regarding the results. Chapter 5 evaluates the thesis study and presents a conclusion.

2

Theoretical Background

This chapter provides the theoretical knowledge required in understanding the scope of the research. Section 2.1 covers the basic concepts and principles underlying an ultrasound imaging system. Section 2.2 describes the use of ultrasound in the field of breast imaging. Section 2.3 explores studies relevant to the process of designing an ultrasound probe that are available in literature.

2.1. Ultrasound Imaging

The term ultrasound is used to describe sound waves with frequencies that exceed the upper auditory limit of 20 kHz. Ultrasound is used in the medical field as an imaging modality that makes use of the varying acoustic properties of the body to construct an image of the tissue structure. The first use of ultrasound as an imaging modality for medical diagnosis is attributed to Wild and Neal [18] in 1951.

The process of ultrasound imaging is based on the pulse-echo principle. A device called transducer generates a short, spatially-localized pulse (beam) of ultrasound that is transmitted to the patient. As the pulse propagates through the patient's body, a small fraction of the pulse is reflected back to the transducer while the remainder continues to travel along a straight line. The reflection occurs when the pulse encounters an interface of two tissue types of different acoustic properties. Depending on the degree of difference between the two mediums, the pulse may be reflected more strongly at certain points of intersection than others. A collection of these echoes of varying amplitude are gathered overtime and used to display an amplitude versus time record. This type of display is commonly referred to as *A-mode* (or A-line, A-scan), with *A* denoting amplitude. When the system consists of an array of transducer elements, a group of these A-lines are gathered and ultimately used to create an acoustic image ultimately used to create an acoustic image of the underlying tissue structure. Each vertical line in the image is composed of varying degrees of brightness, which correspond to the echo amplitude in an A-line signal. This is called a *B-mode* display, with *B* representing brightness.

2.1.1. Physics of Ultrasound

Speed of sound varies in different types of tissues. The average velocity (c_0) at which ultrasound travels through biologic tissues is approximately 1540ms^{-1} [19]. A medical ultrasound device typically assumes this value to compute for the depth at which echoes were generated. This means that in order to determine the localization of an echo generated at time t , Equation 2.1 is used. The division by two is to account for the fact that the pulse needs to travel twice the distance as it begins its path at the transducer, reaches the tissue boundary, and is reflected back to the transducer.

$$D = \frac{t \cdot c_0}{2} \tag{2.1}$$

As briefly mentioned above, echoes are generated when the ultrasound pulse meets a boundary between two tissues of differing acoustic properties. The most important property that defines the interaction of ultrasound with tissue is called the acoustic impedance (Z), which in its simplified definition is described in Equation 2.2, where ρ is the density of tissue and c is the speed of sound as it propagates through the tissue. A larger difference between the acoustic impedance of the two tissues results in a higher intensity (I_r) of the reflected pulse. Equation 2.3 shows its mathematical expression, where Z_1 and Z_2 are the acoustic impedance of each tissue type. This equation only applies when the angle of incidence is 90° .

$$Z = \rho \cdot c \quad (2.2)$$

$$I_r = \left(\frac{Z_2 - Z_1}{Z_2 + Z_1} \right)^2 \quad (2.3)$$

Specular reflection, which occurs when there is a difference in the acoustic impedance of two adjacent mediums, is not the only interaction that happens in ultrasound propagation. If the angle of incidence is not 90° , a *refraction* occurs, where the transmitted pulse undergoes a change of direction in its travel. *Scattering* takes place when small particles within the tissue, whose dimensions (x) are smaller than the ultrasound wavelength ($x \ll \lambda$), bring about the diffused reflection of the pulse in multiple directions. Most of the signal visible in ultrasound images are products of scattering [20], which is what forms the distinctive texture in the images. The roughness of the surface at which two types of tissues meet also contribute in the differing behavior of the ultrasound beam. *Attenuation* refers to the decrease of intensity of the ultrasound pulse as it travels through tissue. *Absorption* describes the loss of acoustic energy as the conversion to heat occurs.

There exists a trade-off between resolution and depth of penetration that largely depends on the the frequency that the ultrasound transducer operates on. The higher the frequency, the better contrast resolution in the resulting signal [21]. Optimal contrast resolution is important in the differentiation of solid masses from the surrounding tissue [22]. The presence of lesion is sometimes identified through subtle variations in the echo response. On the other hand, higher frequencies also result in greater attenuation and therefore weaker echo signals at higher depth values. This increases the difficulty of analysis for deeper tissue structures. Thus, operating frequency of an ultrasound equipment is selected based on the application for which it is used. In breast imaging, the frequency used is usually between 7 to 10 MHz [23].

2.1.2. Ultrasound Transducers

An ultrasound transducer converts electrical energy into sound waves that are transmitted to the patient, and as echoes are produced, converts the reflected sound waves back into electrical energy. Typically, it consists of a piezoelectric material, which has a property that induces mechanical vibrations through the applying of electrical signals and vice versa. Modern ultrasound equipment commonly makes use of an array of transducer elements as for B-mode display of the tissue structure. Implementation of an ultrasound imaging system in B-mode requires an understanding of array beamforming. However, this topic is outside the scope of this study, which focuses on the use of single-element transducers.

The shape of an ultrasound transducer may be either circular or rectangular, and it may also have either a flat or curved form. A flat form makes for an unfocused transducer, while a curved one makes for a focused transducer. Focusing the transducer allows it to produce narrow ultrasound pulses, resulting in a higher lateral resolution, which is related to the ability of the system to discern objects in the lateral direction (perpendicular to the direction of the beam). An acoustic lens may also be used on a flat transducer to focus its ultrasound beam.

2.1.3. Beam Profile

Ultrasound beams have a width that varies in function of distance from the transducer. As depicted in Figure 2.1, this width variation forms a profile that exhibits two different patterns: a converging beam of a certain length (Fresnel zone), followed by an infinitely diverging beam (Fraunhofer zone). For unfocused transducers, the length of the near field, also known as the Fresnel zone, is a function of the radius (r) of the transducer

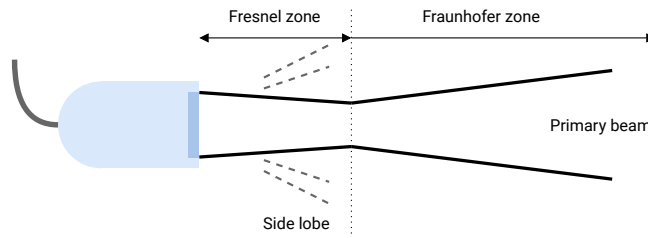


Figure 2.1: Ultrasound beam profile of an unfocused, single-element transducer (reproduced from [20]).

and the wavelength (λ) of the sound wave. The relationship is shown in Equation 2.4, from which it can be deduced that larger frequency and physical transducer diameter result in an increased near field length, which leads to a better lateral resolution.

$$\text{Near Field Length} = \frac{r^2}{\lambda} \quad (2.4)$$

Side lobes are unwanted emissions of ultrasound energy that travel away from the main beam axis. They are typically have a much weaker intensity than the primary ultrasound beam but still pertain the ability to cause artifacts in the resulting image. The emissions of side lobes may be reduced by using a small value for the width of the transducer element. A typical value used for the width of the element is 1.3 wavelengths (λ), to keep it narrow while still allowing it to have a wide field of view [24].

2.1.4. Signal Processing

The signal processing steps that are usually used in an ultrasound imaging system are briefly summarized in Figure 2.2. The evolution of how the signal looks after every processing step is displayed in the figure. The details of each step are described in the following paragraphs. These methods are not always the same for each imaging system, as there are many different techniques that may be introduced in the processing, which are discussed in Subsection 2.1.6.

Echo Detection

Echoes are received at the transducer in the form of radio-frequency (RF) signals. After their reception, these echoes need to undergo several signal processing methods. For multi-element transducers, the process begins by applying appropriate weights to the received echoes to account for the beamforming delays and then summing the results. This step is not used for single-element transducers operating in A-mode.

Time Gain Compensation

In order to compensate for the effects of acoustic attenuation through absorption and scattering, which causes reflections at the deeper region from appearing to have a weaker amplitude in the recorder signals, a simple correction called time gain compensation (TGC) is applied. This correction is taken from [25] and is expressed in Equation 2.5, where X and Y represents the signal before and after the correction, respectively. It assumes that absorption decays as a function of penetration depth (z) in cm, transmit frequency (f) in MHz, and attenuation coefficient (α) in $\text{dB MHz}^{-1} \text{ cm}^{-1}$.

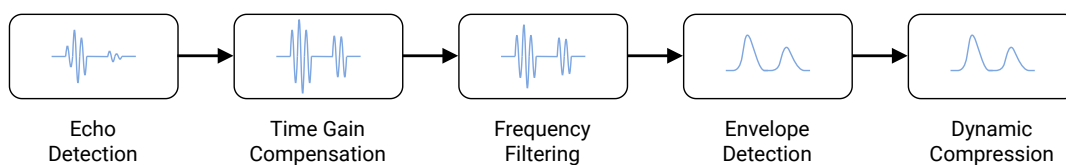


Figure 2.2: Signal processing methods for the received echoes

$$Y = X \cdot e^{-\alpha 2zf} \quad (2.5)$$

Frequency Filtering

The purpose of this step is essentially noise rejection, which in other words has a function to remove a significant amount of undesirable noise outside the transmitted frequency range that may be generated from scattered pulses. In the simplest form, this may be realized through the use of a Gaussian filter centered about the transmit frequency.

Envelope Detection

This processing step involves two parts: (1) rectification, where the portion of the signal that has a negative amplitude is inverted to positive values; (2) envelope detection or demodulation, which converts the rectified signal into a smoothed single pulse.

Dynamic Compression

The dynamic range, or the effective range of operation of an electronic device, of the processed echo response is often too wide to be visually perceived when converted into a grayscale image. This is then reduced by using a logarithmic function.

2.1.5. Acoustic Artifacts

It is important to note that acoustic information of a medium provided as a result of an ultrasound scan represents the real values in full accuracy. Ultrasound-generated artifacts are normally present in the results of a scan. Artifacts are defined as perceived deformation, error, or addition that appears as a result of the instrument of observation. Acoustic artifacts are the error in presentation of ultrasound information [26]. They are also commonly referred to as imaging artifacts, as they usually discussed in terms of 2D acoustic images, and therefore have a more visual description. One of the goals of this thesis is to investigate whether some of the artifacts, that are often used as a defining characteristic in malignancy detection of breast masses, are discernible in the one-dimensional scan lines produced by single-element transducers. Some examples of acoustic artifacts are described in the following paragraphs.

Speckle

The granular texture that is easily noticeable in sonographic images is defined as a speckle. It is undesirable because it reduces image contrast, which is the ability to recognize a structure against a background, while also making it more difficult to distinguish between subtle gradations and boundaries in tissue structure. The effect of speckle can be quantified using a metric called contrast ratio (CR), which is simply defined as the average gray-scale level of brightness in the object (usually a cyst) compared to the tissue that surround it [25]. The equation for contrast ratio is shown in Equation 2.6, where A_{in} denotes the average amplitude of the signal in the object and A_{out} denotes that in the surrounding area. A value close to 0 indicates poor contrast, while those closer to 1 means good contrast.

$$CR = \frac{A_{out} - A_{in}}{A_{out} + A_{in}} \quad (2.6)$$

Acoustic Shadowing

When the deeper tissue seem less echogenic than normal, caused by a smaller attenuation coefficient that it has compared to the structure that lies closer to the surface of the skin. In a 2D image, acoustic shadowing appears as the a dark region (shadow), posterior to a structure. The appearance of acoustic shadowing behind a mass in an acoustic image of the breast is often an indication of malignancy [27]. An example of how acoustic shadowing appears in a B-mode image is shown in Figure 2.3.

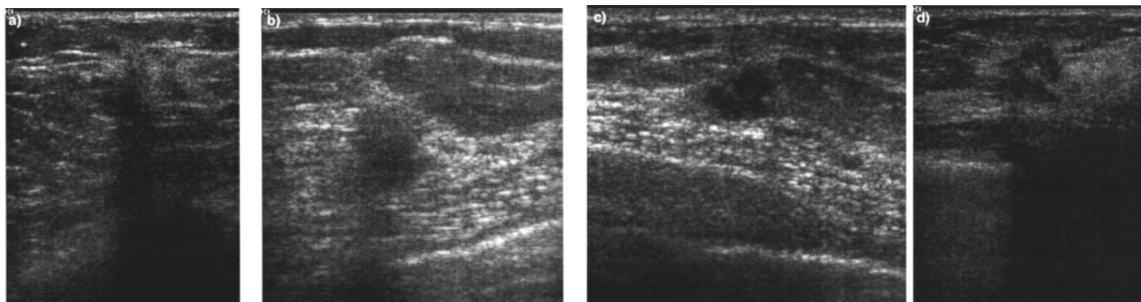


Figure 2.3: Various sample images of malignant lesion that exhibits a certain level of acoustic shadowing: (a) substantial acoustic shadowing; (b) lesser acoustic shadowing; (c) no acoustic shadowing; (d) overshadowing due to an artifact. Images taken from [28].

Overgain and Undergain

Proper gain settings need to be applied in the post-processing of the output signal. Using values that are inappropriately low may lead to the absence of a structure in the final image (image generally appears too dark), while those that are inappropriately high would conceal existing structure (image generally appears too bright). In a machine for an ultrasound imaging system, the gain values related to time gain compensation and dynamic compression are adjustable by the sonographer using a physical slider.

2.1.6. Advanced Processing Methods

Tissue Harmonic Imaging

This refers to the use of a frequency filter that is centered at the higher harmonic, whose value is an integral multiple of the fundamental frequency [20]. Normally, the second harmonic is used. Ultrasound waves are distorted as they propagate through tissue, they typically start as a perfect sinusoid shape and transforms into a sharper, more triangular waves. These sharper waves contains frequencies that are centered around the higher-order harmonics. This means that tissue harmonic imaging allows for better imaging at greater depths.

Spatial Compounding

Spatial compounding is a technique that electronically steers ultrasound beams from a multi-element (B-mode) transducer, by varying the orientation of the ultrasound beams, such that the same tissue region may be scanned multiple times [20]. Several images are then obtained and eventually combined together to create a single image. The technique is known to reduce speckles, noise, and other artifacts.

Frequency Compounding

This method involves assigning a weight to several different sub-band images, which were obtained by passing the beamformed ultrasound signal through a bandpass filter. The weight value is based on a certain spectral weighting function. The multiple images are then summed to generate a final image. Frequency compounding is normally used to reduce speckles [25].

2.2. Ultrasound for Breast Imaging

Ultrasound, along with mammography, is now the most important imaging modality used in screening of breast cancer. As discussed in the previous chapter, it yields a comparably high diagnostic value.

Breast is composed of several different types of tissues, with each type having unique density and speed of sound values. An anatomy of the breast is shown in Figure 2.4 (not all types of breast tissue are shown). Structural composition of the breast varies greatly from woman to woman, evaluated through various aspects that include volume, fat composition, skin thickness or degree of branching. This variation is caused by factors such as age of the person, whether they are nulliparous (have previously given birth) or not, the

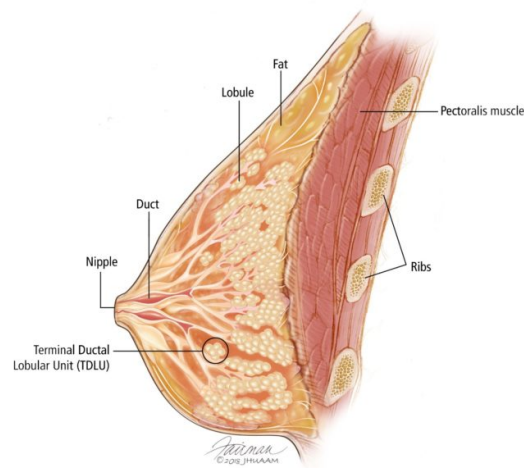


Figure 2.4: Anatomy of the breast [31].

phase of menstrual cycle in fertile women and menopausal status [29]. The structural composition of the breast affects the way an ultrasound pulse interacts with the tissue during an ultrasound scan. Ultrasound imaging has a lower diagnostic values for breasts that have sustained involution, where glandular elements are replaced collagen and fat [5]. The risk of involution increases with age [30]. Aside from this, the thickness of breast skin also varies depending on the age and fertility of the person. The value ranges between 0.5 mm to 2 mm for younger people and increases with age [5].

When an abnormal mass is found in breasts, it may manifest itself in the form a cyst, which is a pocket of membranous tissue that contains a substance such as fluid or air, or it may have a solid structure. The mass could also be classified as either benign (non-cancerous) or malignant (cancerous). A cystic lesion, such as simple cysts, fat necrosis, oil cysts, galactoceles, or breast abscess, is usually of benign nature, albeit this is not always the case. Different types of benign solid lesions include fibroadenomas, phyllodes tumours, hamartomas, lipomas, among others. According to Sencha et al. [5], fibroadenomas account for 95% of all benign breast masses, while the most common malignant breast disease is invasive ductal carcinoma (59%), followed by invasive lobular (8%), tubular (7%), cancer in a cyst (5%), mucous (4%), and others (13%). Most cancers are developed from the cells which make up the lobules and terminal ducts. Invasive ductal carcinoma is usually situated around the TDLU tissue [32].

2.2.1. Characteristics of Breast Masses

With the large number of breast diseases that exist, there is no specific, single feature that could be used to predict malignancy of a breast mass. However, certain features are quite prevalent in the differentiation. A benign breast mass tends to have a round or oval shape (94%), circumscribed margins (91%) and a width-to-AP¹ ratio of higher than 1.4 (89%). On the other hand, a malignant breast mass is more likely to have an irregular shape (61%), spiculated margins (67%), and a width-to-AP ratio of less than 1.4 (40%). A lower width-to-AP ratio means that the object is taller than wider [33, 34]. The size of a breast mass varies between the type of the mass. According to Sencha et al. [5], the dimensions of malignant ones are 0.5–1.0 cm (25%), 1.1–3.0 cm (69%), and larger than 3.1 cm (6%).

2.2.2. Methods for Malignancy Detection

In 1952, with the first use of A-mode ultrasound imaging, Wild and Neal used the area under the plotted echo response to differentiate between malignant and benign tissue [25]. In B-mode imaging, sonographers would analyze the characteristics of the mass that are present in the image and make a diagnosis based on them and their extensive knowledge. The characteristics evaluated also include posterior acoustic shadowing, which is often associated with malignant breast masses [27]. However, the presence of acoustic shadowing does not

¹Anteroposterior

necessarily indicate malignancy, as certain types of benign lesions also appear to produce this artifact [35].

2.2.3. BI-RADS

Breast Imaging-Reporting and Data System (BI-RADS) is a system developed by American College of Radiology (ACR) that serves to guide the interpretation of acoustic images produced by an ultrasound imaging system, mammography, or MRI [36]. By providing a standardized reporting and classification system, BI-RADS has improved the communication and reduce confusion, through elimination of ambiguity, within the field of breast cancer screening as well as the research [37]. It has been widely adopted all around the world and used by many screening programs in the United States and Europe [38]. One particular aspect of BI-RADS that is of interest to this study is the classification of breast density levels. There are four categories defined: extremely dense, heterogeneously dense, scattered fibroglandular densities, and almost entirely fatty.

2.3. Related Work

Due to a large number of factors involved, designing a probe in an ultrasound imaging system is a difficult and challenging task. For clarification purposes, even though in practice the main physical device is often called as the transducer, in this thesis we will stick to the definition of transducer as stated in Subsection 2.1.2, which is the component of the device that transmits and receives ultrasound waves. The physical device itself will be referred to as an ultrasound probe, which contain the transducers.

Daft and Leue [39] patented a system that allows its users to select a set of input parameters that define various characteristics of a multi-element probe for B-mode imaging and assess its performance. The system aims to optimize the quality of a probe design in terms of its image quality, as well as other parameters, through statistical means. This means simulating the statistical distribution of quality measures and measuring their sensitivity to changes in the design parameters. In their system, the quality measures that are being considered are related to the visual properties of the sonographic images.

3

Methodology

This chapter details the methodology of this thesis study. Section 3.1 outlines the design of experiment. Section 3.2 discusses several breast models that have been used in breast imaging studies. Section 3.3 examines the different acoustic software that are available for use. Justifications for why a certain tool is chosen for this thesis is provided in both sections. How the simulation is arranged is detailed in Section 3.4. Section 3.5 lists the input parameters and boundary conditions of the experiments, and which values are used. Section 3.6 describes how the performance of the input parameter values are evaluated based on the experimental results. In Section 3.7, how the simulation tools are used together are explained.

3.1. Design

The investigation will be carried out through a series of experiments in a computer-simulation environment. Besides the lack of relevant datasets that could be used for the study, one main advantage of computer-simulation studies is that it allows the possibility to systematically and comprehensively explore the parameters of a system, something which is generally impossible through actual experimentation. In the field of medical imaging, simulation studies are evidently more efficient as it removed the need to gather a very large number of patients with varying pathology.

There are two components that are instrumental in the realization of the simulation: numerical breast models and simulated propagation of acoustic wave. An important remark to be noted is that this study forgoes the details of the architecture of an actual transducer that would normally include necessary elements such as the beamformer, acoustic absorber, and damping block.

3.2. Numerical Models

Due to the importance of computer-simulation studies in the emerging field of imaging technologies, various numerical breast phantoms are readily available in literature. They are necessarily, anatomically realistic, although in reality the degree at which a certain model represents reality varies greatly. Many existing models simplify the naturally-complex anatomical structure of breasts. Numerical breast phantoms are usually stored as a 3D volume data, where each point in the structure represents a type of tissue. The models can be constructed through various means.

OA Breast Database [40] consists of 3D numerical breast phantoms that were generated from clinical contrast-enhanced MRI data. This data is fed into a framework that extracts its vessel structures and then processed to segment different types of tissue within the breast. There are four types considered: blood vessels, skin layer, fat, and fibroglandular tissues. The models produced can be assigned with optical and acoustic parameters for use of simulation in photoacoustic and ultrasonic breast imaging. The resolution (voxel grid size) of the generated models are $200\mu\text{m}$. A limitation of this framework is that the MRI scans were per-

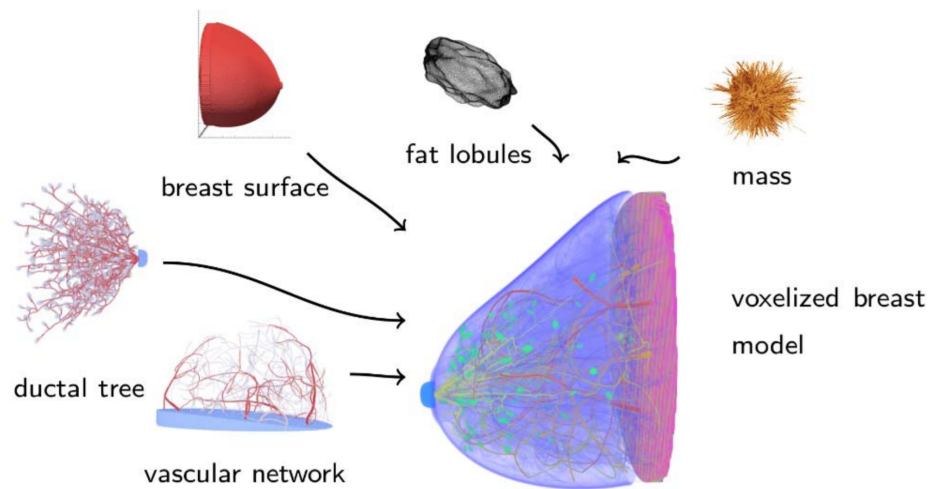


Figure 3.1: Anatomical components of the simulated breast model [43].

formed on healthy patients, and therefore abnormal breast masses are not considered in the generated digital models.

OpenVCT [41, 42] offers a pipeline for Virtual Clinical Trial (VCT) for simulations of mammography and digital breast tomosynthesis. The framework of OpenVCT emulates the steps of virtual clinical accrual that in the end generates a database of breast models as well as the reports of their imaging. One component of the framework called OpenVCT Designer, allows the specification of several anatomical features of the breast, with optional insertion of lesions. The breast phantom generator is implemented using an efficient octree-based partitioning algorithm for creation of high resolution anthropomorphic breast models. The resolution of the breast phantom models can be as low as $25\ \mu\text{m}$. The software and resources for OpenVCT are no longer publicly available.

Virtual Imaging Clinical Trial for Regulatory Evaluation (VICTRE) trial [43] was developed at the United States Food and Drug Administration (FDA) to simulate a clinical trial that would normally use human patients. The computational pipeline of VICTRE consists of several components, which include an anthropomorphic breast phantom and breast mass model generators.

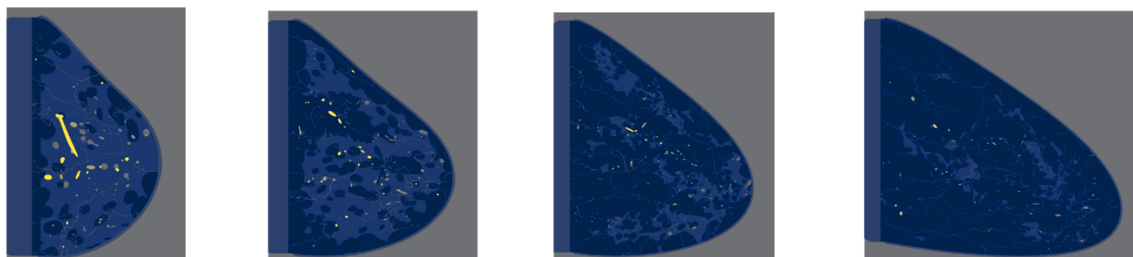
The breast phantom models are created through a procedural analytic method [44]. This method is based on knowledge of breast physiology such that the generated phantom models are able to capture a fair degree of variability to features that are relevant to breast imaging. There are ten types of breast tissues that are considered in the models: skin, nipple, fat, inter-lobular glandular tissue, chest muscle, the suspensory ligaments of Cooper, lactiferous duct, terminal duct lobular unit (TDLU), artery and vein. The assignment of the tissue types in the model makes use of the Voronoi technique, Perlin noise, and tree-generation functions. There are over 200 parameters that can be varied in the software, although most of them require no adjustments in typical situations. The resulting models are multi-modal and are therefore suitable for use in various types of imaging studies, including ultrasound.

The breast mass generator uses a procedural generation method [45], which involves a modified stochastic Gaussian random sphere model that is able to replicate a tumor mass. The mass models produced from this software differ from those from other studies in their fine details. The generated masses are realistic with spicules surrounding their central area, a typical characteristic of a cancerous breast mass. This complex spicule structures are achieved through an iterative fractal branching algorithm. The software allows for variations in the input parameters, including the ones related to the amount of spiculations. The mass generated is later inserted into the breast phantom model. The different anatomical components generated by VICTRE's breast phantom and mass generator software is shown in Figure 3.1. As seen in the figure, other than the structural composition, this parameter also affects the volume and shape of the final model.

The breast phantom and mass model generators in VICTRE is ultimately used in this thesis study mainly due to its flexibility, high resolution, and high accuracy. Both software are open-source, as they let the user

Fat Fraction	
Extremely dense	0.40
Heterogeneously dense	0.66
Scattered density	0.85
Fatty	0.95

Table 3.1: Varying fat composition in each breast category.



(a) Extremely dense (b) Heterogeneously dense (c) Scattered fibroglandular density (d) Almost entirely fatty

Figure 3.2: Side view of the simulated breast phantoms, where the darker blue area denotes fat tissue.

specifies all of the parameters, and are also compatible with the acoustic software used. The sources of the all the VICTRE components are publicly available on GitHub.

3.2.1. Breast Phantom Models

As discussed in the previous chapter, characteristics of human breasts differ between patients. The most defining breast property, within the field of ultrasound imaging, is the density or the fat content of the breast, as it affects the way an ultrasound pulse interacts with matters as it travels through tissue. In order to reflect this variety in the simulated models, certain parameters in the breast phantom generator are slightly varied.

The breast density categories defined BI-RADS are used to create the different breast phantom models. There are four categories of breast composition defined in BI-RADS: extremely dense, heterogeneously dense, scattered fibroglandular densities, and almost entirely fatty. The parameter that is being varied is the fat content percentage. The values used for each density category are taken from [43] and shown in Table 3.1. These values correspond to a quantitative assessment of the BI-RADS categories performed in [46], in which radiologists agree on the following ranges of density for each category: 60.1%–87.9% for extremely dense, 15.9%–82.2% for heterogeneously dense, 1.2%–52.7% for scattered fibroglandular densities, and 0.5%–19.2% for almost entirely fatty breasts. The median is used for the last two categories, while a value closer to the upper limit is chosen for the first two categories. The fat fraction is the complement of the density value.

Although the resolution used in the original VICTRE study is $50\ \mu\text{m}$, this value will result in a very large file size of the models and consequently an extremely long simulation time. Thus, the resolution used in this thesis study is $100\ \mu\text{m}$. Additionally, for simplicity, the other parameter values remain constant for all of the categories. For example, although thickness of the breast skin typically varies from person to person, the skin is imagined as a homogeneous echogenic layer of $0.75\ \text{mm}$ thickness for all categories. A side view of the generated breast phantom models are displayed in Figure 3.2.

3.2.2. Breast Mass Models

Two models of breast masses or lesions will be inserted into the breast model to replicate both a disease of benign and malignant nature. Since a cystic lesion might vary in terms of the substance that it contains, in addition to the fact that fibroadenoma (solid lesion) is the most common benign breast disease, the simulated benign



Figure 3.3: Simulated breast masses



Figure 3.4: Ductal trees in the breast model

mass assumes a solid structure. This mass has features that are commonly identified in a benign breast mass, such as a round and lobulated shape. The simulated malignant breast mass is also attempted to replicate the most common type of malignant breast disease, ductal carcinoma, which is a solid lesion with an irregular shape and spiculations on its surface. The two simulated breast masses can be seen in Figure 3.3. The acoustic parameters used for the benign and malignant mass are different and stated in Section 3.5.

As breast diseases typically start to form at the terminal ductal lobular unit (TLDU) tissue, the simulated masses will be placed precisely at a location where the tissue is segmented to be of the TLDU type. Figure 3.4 shows the ductal trees within one of the breast models. The TLDU is tissue at the end of each branch. This means that there are multiple possible locations for the breast mass to be placed, and therefore allows this thesis study to explore the behavior of the ultrasound probe when the breast mass is located deeper within the breast tissue (further from the skin surface). As for the size of the simulated masses, the value at the lower limit of the normal range is used (diameter of 5 mm). The reason for this is to provide the worst case scenario, as smaller structures are more difficult to distinguish in an ultrasound scan. The simulated mass has the same resolution as the breast phantom model.

3.3. Acoustic Wave Propagation

There exist several different software that can be used to model wave propagation in acoustics, some of which are summarized in Table 3.2 and described in the following paragraphs.

Field II

Field II [47] is an ultrasound simulation program that uses the Tupholme-Stephanishen method to calculate for the pulsed ultrasound fields using spatial impulse responses [48, 49]. However, a major concern related to this software is computation time.

Field II	Focus	Ultrasim	k-Wave
MATLAB/C	MATLAB	MATLAB	MATLAB/C++
Freeware (Closed-source)	Freeware (Closed-source)	GNU GPL	GNU LPGL
Spatial impulse response	Fast nearfield method	Discrete Rayleigh integral	k-space pseudospectral method

Table 3.2: Comparison of the available acoustic modeling software

FOCUS

FOCUS [50] implements the Fast Nearfield Method to calculate for the ultrasound pressure fields. The Fast Nearfield Method (FNM) [51, 52] removes the singularity from the impulse response expressions to allow FOCUS to achieve high accuracy and fast computation time. FOCUS also solves some problems that have been found in the results of simulations with Field II. FOCUS has several functions that allow its user to create the propagation medium using a predefined structure, and cannot use medium structures that have been produced externally.

Ultrasim

Ultrasim [53] computes for the sound fields using discrete Rayleigh integral, implemented as a MATLAB toolbox. Its main use is for exploration of transducer geometry and design of transducer arrays. This toolbox is only able to handle 1D, 1.5D, and 2D transducer arrays and is not compatible for use with voxelized breast phantom models, such as those generated using VICTRE's breast phantom generator.

k-Wave

Possibly the most widely used simulation tool in the field, k-Wave [54] is an open-source MATLAB toolbox for acoustic modeling, developed by Bradley Treeby and Ben Cox from the University College London, and Jiri Jaros from Brno University of Technology. k-Wave is used for time-domain simulation of acoustic wave propagation, both linear and nonlinear, in 1D, 2D, and 3D. It also accounts for power law acoustic absorption and an arbitrary distribution of heterogeneous material parameters. The numerical model is based on a generalized form of the Westervelt equation [55], solved using a k-space pseudospectral method [56]. k-Wave has an advantage in terms of performance as the numerical model that it uses requires a smaller number of spatial and temporal grid points compared to those that are based on finite-difference time domain (FDTD) schemes. Additionally, k-Wave allows the use of MATLAB's Parallel Computing Toolbox and a GPU that vastly decreased the computation time. In the absence of a GPU, k-Wave also provides a more optimized version of the k-space computation function written in C++. k-Wave can be used compatibly with the breast phantom models generated from other software. Thus, in combination with models produced from VICTRE's breast phantom and mass generation software, k-Wave will be used to model the ultrasound wave propagation.

3.4. Simulation Layout

k-Wave only supports linear placements of transducers. This means that in order to position an ultrasound probe as depicted in Figure 3.5a, the model needs to be rotated such that Figure 3.5b is achieved. This position is chosen as it reflects a probable way of placing an ultrasound probe in reality. Since the breast phantom models are stored as raw binary data (8-bit unsigned integer) containing the tissue type of each point in the voxelized breast model, rotating the model simply implies a 3D matrix rotation in a euclidean space (\mathbb{R}^3).

Because of the orientation at which the breast models are generated, the desired placement of the transducers are along the x-axis, as seen in Figure 3.5b. This means that the breast models need to be rotated at the z-axis by a certain degree, such that a portion of the skin surface is relatively parallel to the x-axis. The value

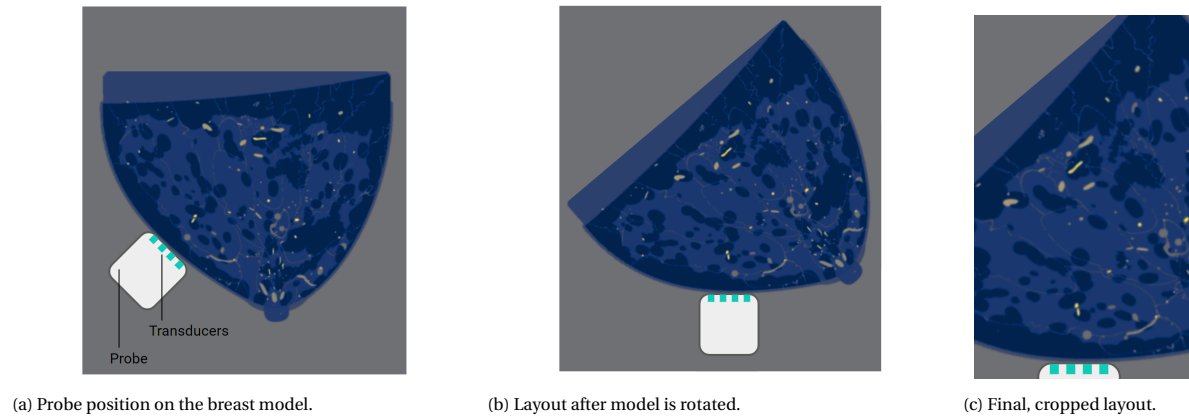


Figure 3.5: Desired position of the ultrasound probe (top view).

of the rotation angle (θ) varies per model. For a breast model \mathbf{B}_0 , a rotation of θ degree around the z-axis is expressed in Equation 3.1.

$$\mathbf{B}' = \mathbf{B}_0 R_z(\theta) \quad (3.1)$$

where R_z is a rotation matrix in the z-axis,

$$R_z(\theta) = \begin{bmatrix} \cos \theta & -\sin \theta & 0 \\ \sin \theta & \cos \theta & 0 \\ 0 & 0 & 0 \end{bmatrix} \quad (3.2)$$

The rotation operation causes a staircase effect on the breast phantom model due to the nonlinear components of the rotation matrix. The original breast model produced by the software \mathbf{B}_0 contains elements b such that b is always one of the 12 distinct values, each representing a tissue type. However, after applying a rotation, \mathbf{B}' contains elements b' where b' is any value in $[0; 255]$ (all possible values of 8-bit unsigned integer). This is an issue as there is only a definite number of tissue types. To eliminate this problem, the elements of the rotated breast model \mathbf{B}' is interpolated using a spline interpolation of order 0, after which all elements of \mathbf{B}' are always one of the 12 distinct values.

The generated breast model that is smallest in size is that of the extremely dense category, with dimensions $505 \times 896 \times 717$ voxels (316 MB). This is already a considerably large file to be opened in MATLAB and it would take hours to compute for a pulse-echo response of a single transducer in its full size. Therefore, it is necessary to crop the 3D volume to extract a region of interest (ROI). An example of the cropped model is shown in Figure 3.5c. All four of the breast models are cropped to be of dimensions $300 \times 500 \times 500$, or equivalent to $30 \times 50 \times 50$ mm. This allows for a maximum input frequency of up to 7.1 MHz to be simulated in k-Wave.

3.5. Simulation Parameters

3.5.1. Input Parameters

There are three input factors that will be investigated:

- (a) **Number of transducers:** This is the number of single transducers, operating in A-mode, that will be used concurrently with each other.
- (b) **Distance between transducers:** The distance at which each transducer will be placed from each other.

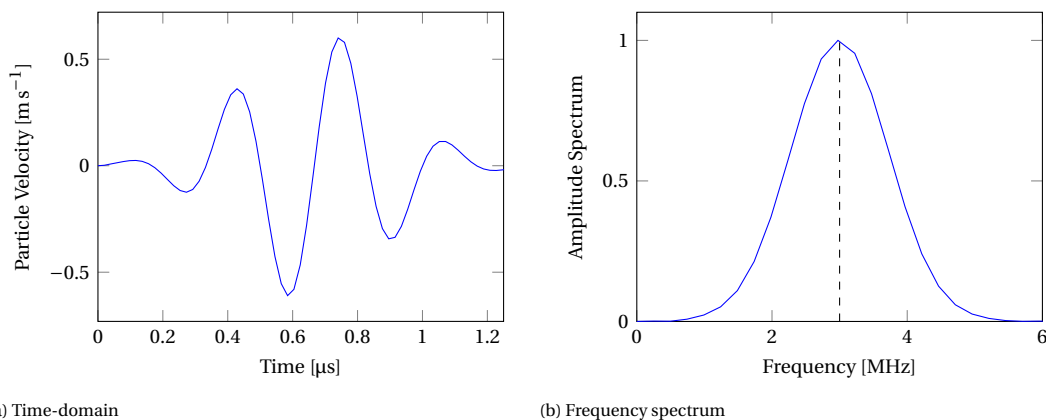


Figure 3.6: Input signal

- (c) **Input frequency:** The center frequency of the transmitted ultrasound pulse. Although ultrasound for breast imaging typically uses a value between 7–10 MHz, performing simulations with values that high will take a very long time to finish. The values tested will be restricted to below 7 MHz (also the maximum allowed by k-Wave based on the computational grid size). The next subsection provides more details on the input signal.

3.5.2. Boundary Conditions

The following are the constant parameters with which all simulations are performed.

Simulation Grid

- (a) **Grid size:** The size of each voxel in the computational grid is essentially the resolution of the breast model, which is equal to 100 μm .
- (b) **Layout size:** As mentioned in the previous section, all the breast models are processed to finally have dimensions of $300 \times 500 \times 500$ voxels. These values are large enough to allow for frequencies of up to 7.1 MHz to be simulated, while also small enough to have a reasonable computation time. Computation time is important as a large set of experiments need to be executed.

Transducer

- (a) **Dimension of Transducer** Each transducer element has the shape of a rectangle with of width 1.3λ and length 0.8 mm. The width value is chosen based on literature, while the length value is chosen as an arbitrarily small number that is almost always in proportion with the varying width.
- (b) **Perfectly Matched Layer (PML)** in the computation has the size of $1 \times 1 \times 1$ mm.

Input Signal

The input signal used to excite the transducer element is a tone burst of four cycles, centered at a frequency defined by the third input parameter. The input signal is displayed in Figure 3.6.

Acoustic Parameters

The acoustic medium parameters of the breast tissue, which include the speed of sound (c) and density (ρ), are collected from literature [25, 57–59]. The values in different studies may differ with one another, in which case the median value is taken. The values used in the simulation are listed in Table 3.3.

Tissue	c ms^{-1}	ρ kgm^{-3}
Water ¹	1482	1000
Fat ²	1420	928
Skin ³	1610	1200
Glandular ²	1560	1040
Muscle ¹	1580	1041
Ligament ²	1560	1050
Duct ²	1540	1032
Artery ²	1570	1063
Vein ²	1559	1056
Benign Tumor ^{4,2}	1513	1060
Cancerous Tumor ^{4,2}	1548	1060

Table 3.3: Acoustic parameters used in the simulation (¹[25] ²[57] ³[58] ⁴[59]).

3.5.3. Signal Processing

The signal processing of the output of the simulated ultrasound propagation, which is the detected echo at the transducer, follows the steps as described in the previous chapter. An example of how this looks is shown in Figure 3.7. A time gain compensation function is first applied to the detected echo. The signal is then filtered using a simple Gaussian frequency filter to remove noise. An envelope detection is now applied to the signal, after which it is compressed using a logarithm function. The output of this step is the final output used in the analysis. Both the time-gain and compression values are not constant for all simulation results. Instead, the values are manually adjusted. This is explained further in the next chapter.

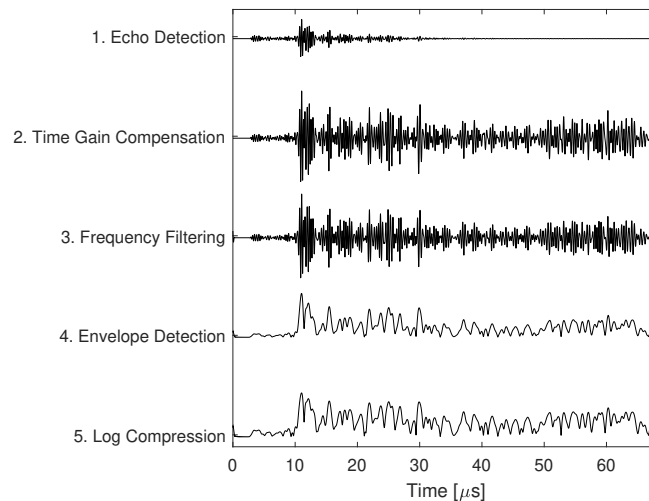


Figure 3.7: Signal processing steps executed on MATLAB

3.6. Design Requirements

Designing a transducer requires a set of criteria to guide the process. To evaluate a certain configuration of an ultrasound probe, its measured response will be compared in the breast models of different density level.

Each configuration will also be tested for breast models that contain both a benign and malignant mass. However, not all configurations of input parameters will be run on all levels of density. This is mainly due to the large amount of time that one simulation takes to finish. When it seems evident from the results that an effect that is observed with a certain breast type will persist in the other types, it would be redundant to repeat the experiment. Regarding the analysis of the output, contrast ratio (CR), as discussed in the previous chapter, will be used as a method to compare the performance of the parameter value with respect to other values. It was considered a possibility to define a fixed set of design requirements in terms of the breast and mass types, with an indication of whether they have been fulfilled according to whether the contrast ratio value is above a certain threshold. However, it would be difficult to pinpoint the exact threshold, and the methods are not available in literature. Therefore, the contrast ratio values would just be compared with each other.

3.7. Computational Pipeline

In order to maximize the computational speed of the process, the pipeline as shown in Figure 3.7 is used. The breast phantom and mass models are first generated using VICTRE's generator software, which were written in C. The generated breast models, which are stored in a raw volume, are manipulated using Python programs for rotation, cropping, and insertion of the masses. The reason for this is purely computational performance, as doing so is much faster than opening and manipulating the data file in MATLAB. Then, after the final layout is obtained, a MATLAB script file reads it and utilizes functions from the k-Wave toolbox to create a k-space numerical model, stored in an h5 file. The k-space pseudospectral function written in C++, distributed in the k-Wave toolbox source code, takes this h5 as input and outputs lines of radio frequency echo data detected at each voxel of the transducer. This output file is fed back into MATLAB on a different script file, which processes it through several signal processing steps to produce the pulse echo (A-line) response of the simulation. MATLAB is also used for analysis of the responses.

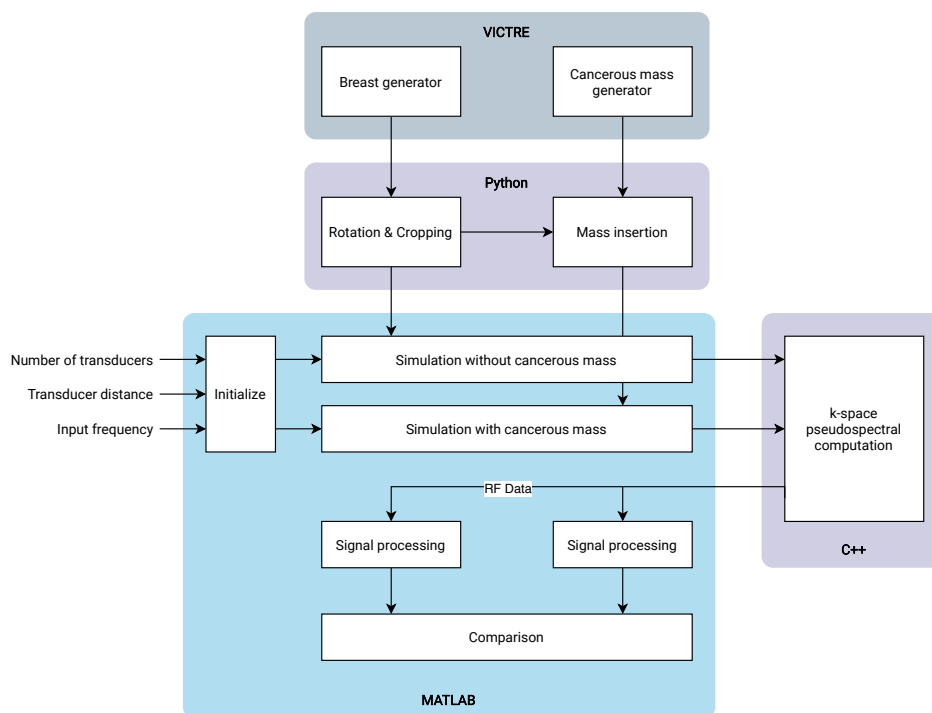


Figure 3.8: General overview of the simulation environment.

4

Experimental Results

This chapter displays and discusses the results of the experiments. In Section 4.1, several preliminary experiments are run in order to demonstrate how ultrasound behaves with different breast and mass types. Section 4.2, Section 4.3, and Section 4.4, respectively contains the results of varying the design parameters: distance between transducers, input frequency, and number of transducers. In Section 4.5, we discuss whether B-mode acoustic artifacts are visible in the results. Section 4.6 explores a new parameter and Section 4.7 briefly describes the unavailability of real data to compare to.

4.1. Preliminary Runs

Two computers are used to run the simulations. A set of simulations is executed in parallel using two computers. The first computer is configured with a Linux OS, Intel Core i7-3770 CPU (3.40 GHz), and 8 GB of RAM where a simulation of a single transducer takes approximately 6500 s and the second computer is configured with the Windows OS, Intel Core i7-6700 CPU (3.40 GHz), and 8 GB of RAM where the simulation is completed in about 9000 s. For a given configuration, one experiment needs three simulation runs (no mass, benign mass, malignant mass) to allow for comparison. Therefore, a single experiment requires up to 27 000 s (7.5 hours), per transducer, to complete.

4.1.1. Basic Settings

To first see how the ultrasound behaves and how the measured response looks like, a simulation was ran with the following configuration: 1 transducer, an input signal with the center frequency of 3 MHz, with a heterogeneous breast model and a benign mass model located 8 mm deep (from the skin surface). The probe is positioned to have its center parallel to where the mass is located. The recorded response over time is shown in Figure 4.1. Since the mass is located 8 mm deep, using Equation 2.1 it can be deduced that the signal should be reflected by the mass around time t ,

$$t = \frac{2D}{c_0} = \frac{2 \cdot 8 \cdot 10^{-3}}{1540} = 10.39 \mu\text{s}$$

This is the point in time where the two responses start to differ, as seen in the plotted graph, while they initially have a very similar shape. Where mass is present, the echo is reflected more strongly here than where mass is not present. This first experiment shows that the transducer is able to produce a different response with the existence of a mass, just as it was expected to behave. Experiments will then be ran with variations in both the type of mass and the density level of the breast model, to demonstrate their effects on the measured response.

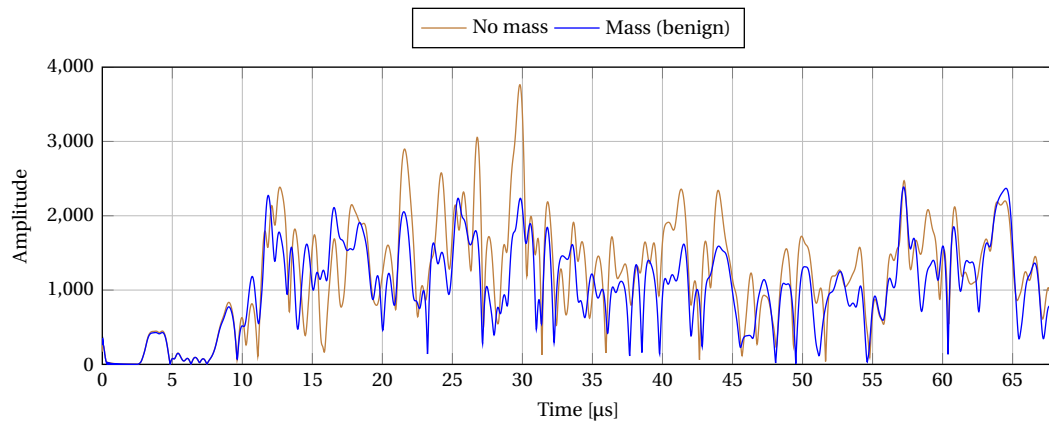


Figure 4.1: Mass vs. no mass results in the time-domain response (1 transducer at 3 MHz, heterogeneously dense breast).

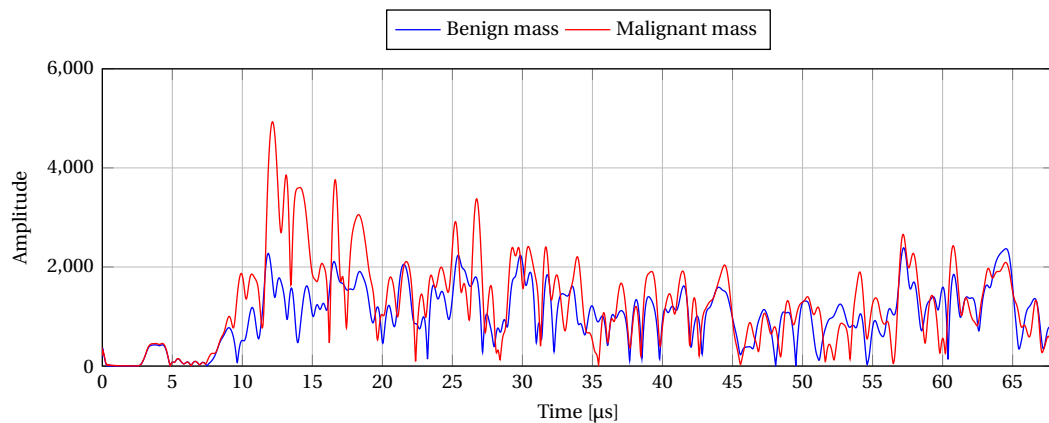


Figure 4.2: Benign vs. malignant mass results in the time-domain response (1 transducer at 3 MHz, heterogeneously dense breast)

4.1.2. Mass Variations

The difference of the response of transmitting the ultrasound waves towards breast tissue that contain a benign and malignant mass are shown in Figure 4.2. The amplitude of the echo at the start, around where the mass is located, is much stronger with the malignant mass. This stark difference could suggest that the echo response may be used to identify the presence of a mass if the amplitude reaches beyond a certain threshold. However, this might not be case for all types of breasts. This will be shown in the next subsection.

4.1.3. Density Variations

Running a set of experiments with the same set of input settings 1 transducer at 3 MHz, for all breast models of the four differing degrees of density level (without mass insertion) generate results as shown in Figure 4.3. It was evident in these experiments that in order to avoid the overgain and undergain artifact, the values for the time gain compensation (TGC) function and the log compression function need to be adjusted accordingly. These adjustments were done manually by looking at the amplitude values in the resulting plot and aiming to have a flat average value. Table 4.1 shows the values used for each breast type. Evidently, the gain value needs to be increased with decreasing density of the breast tissue. This is due to the known fact that the ultrasound wave that is being attenuated more with a higher percentage of fat tissues.

To look at the effect of the density variation of the breast in the ability of the ultrasound to discern a mass from its surrounding tissue, contrast ratio may be used. By defining A_{in} as the average amplitude of the signal in the mass, A_{out} as the average amplitude of the signal outside the mass, and using Equation 2.6, the contrast ratio can be calculated. We know that the mass boundaries in the vertical axis are located at depth 8 mm and 12 mm, which means that A_{in} is amplitude A for $t \in [10.39, 15.50]$. The calculated contrast ratio

	TGC	Compression Ratio
Extremely dense	0.10	3
Heterogeneously dense	0.22	3
Scattered density	0.25	5
Fatty	0.28	5

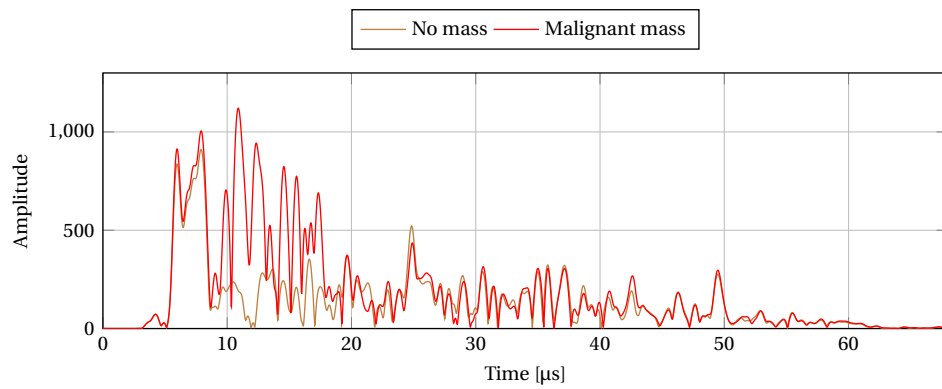
Table 4.1: Gain values

	$A_{in,b}$	$A_{out,b}$	CR_{benign}	$A_{in,m}$	$A_{out,m}$	$CR_{malignant}$
Extremely dense	697.64	495.01	0.1699	1022.12	463.79	0.3758
Heterogeneously dense	1360.80	1017.03	0.1446	2699.02	1137.92	0.4069
Scattered density	2922.52	2770.85	0.0266	4124.93	2599.99	0.2268
Fatty	2914.27	1131.23	0.4408	3047.00	907.04	0.5412

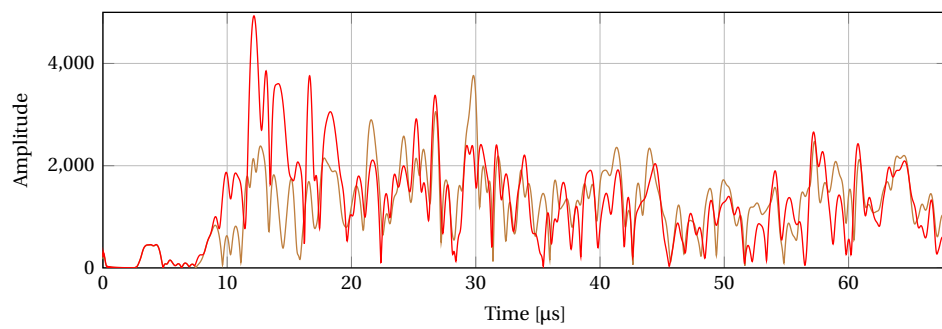
Table 4.2: Mass contrast ratio for each density level

values are shown in Table 4.2. Since a higher value implies a better contrast, this is more desirable than a lower contrast value. Generally, the lesser the density (more fatty), the higher the contrast ratio, except for scattered density. This means that the ultrasound probe performs better in terms of identifying the presence of an abnormal mass when there the breast is less dense. We could also observe in the results that the contrast ratio is stronger in malignant mass. This is most likely due to its spicules and speed of sound, which is higher than that of a benign mass.

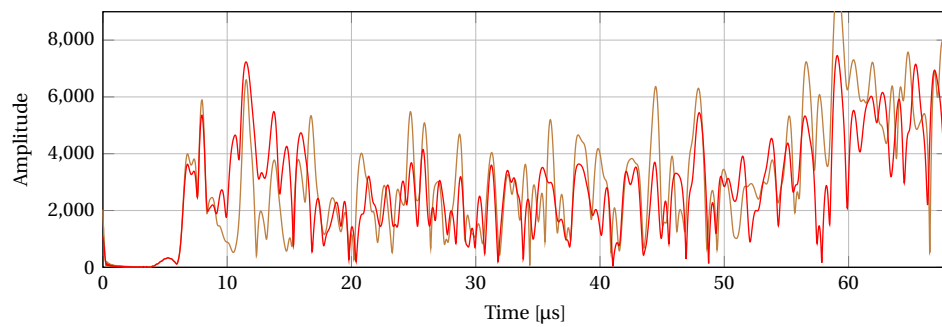
The results of the experiments in this section should be able to help explain the results of the next experiments, as we start the investigation of parameter variations.



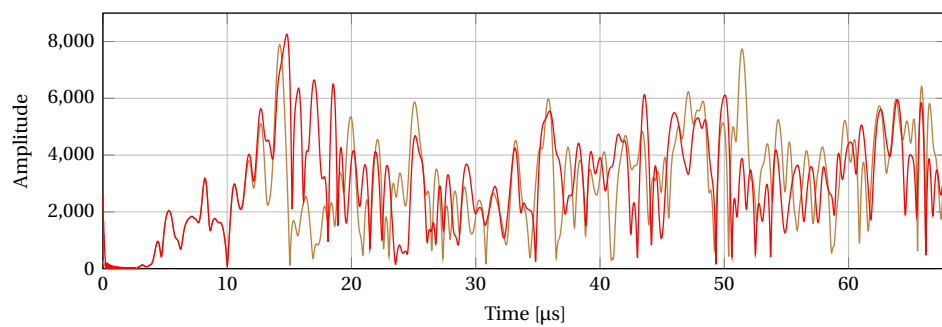
(a) Extremely dense



(b) Heterogeneously dense



(c) Scattered density



(d) Fatty

Figure 4.3: Time-domain echo response for each breast specimen

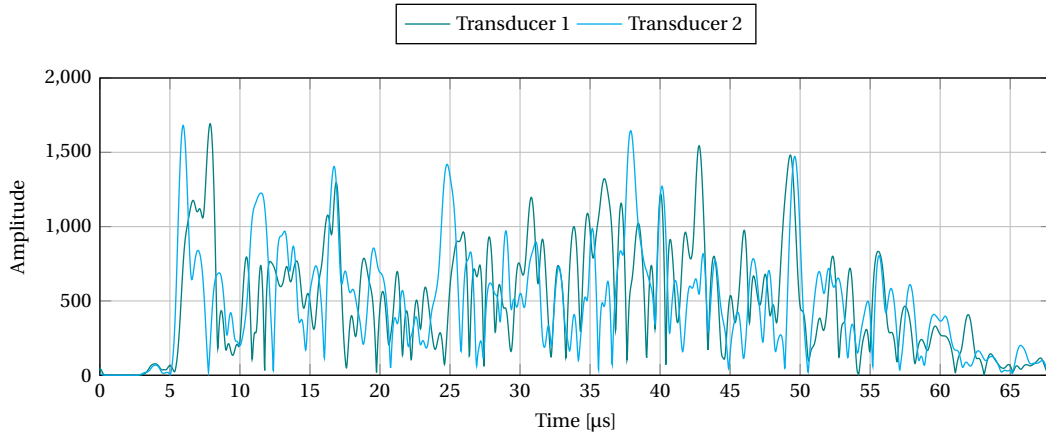


Figure 4.4: Two transducers placed next to each other (extremely dense breast with a benign mass at 3 MHz).

4.2. Distance Between Transducers

When the distance between the two transducers are set to 0 mm, this means that the transducers are placed right next to each other. The result of scan with this configuration, at a frequency of 3 MHz, for extremely dense breast with a benign mass is shown in Figure 4.4. We can observe that the responses are quite different, even though there is no space between the two transducers. This implies that a slight change in the location of the transducer will cause a big difference in the response. This effect also appears at other levels of breast density (see Appendix A.2).

To look at how the distance between each transducer affects the output, a set of experiments are now performed with two transducers, with an increasing distance (s_{tr}) between the two transducers, $s_{tr} \in [0, 1, 2, 3]$ in mm. The calculated values of contrast ratio are shown in Table 4.3 for extremely dense breast and Table 4.4 for heterogeneously dense breast. The configuration of 3 mm yields most of the highest values for both breast models. However, by looking at the tables, we can also discern that the values change in a rather arbitrary manner, from which it can be inferred that there is no correlation between the distance and the response, so long as the value is smaller than the size of the mass (5 mm). Based on this result, it is highly likely that a similar observation will be seen with breast of scattered density and fatty breast, and due to large simulation time required, these breast models were not tested.

Another experiment is ran for the heterogeneously dense breast model with a distance value ($s_{tr} = 7$) that is larger than the mass, which has a diameter of 5 mm. Since the distance is larger than the mass, now neither of the two transducers are facing the mass. It is suspected that the outcome should show that the mass is absent. The calculated contrast ratio values are as follows: $CR_{benign} = [0.1235, 0.1579]$ and $CR_{malignant} = [0.2723, 0.3611]$ for each of the two transducers. By referring back to Table 4.4, it shows that three of the contrast ratio values are the lowest compared to the other experiments with a distance smaller than the mass. This means that there is a much smaller difference between the contrast where the mass is supposed to be compared to the rest, which could imply the absence of the mass. However, it is important to note that we were able to deduce so as other experiments had been completed with smaller distances. When placed in an isolated context where this was the sole scan performed on a breast, it would be much more difficult to distinguish the presence of the mass.

4.3. Input Frequency

To examine the effect of the center frequency (f) of the transmitted pulse, a series of experiments are completed with $f \in [4, 5, 6]$ and f in MHz. The breast model used is of the heterogeneous density and only one transducer is configured. The resulting echo graphs are shown in Figure 4.5. The response shows that at the start of the echo response, there is a peak that increases in amplitude as the frequency is increased. The exact cause for this is not known. However, as mentioned in Chapter 2, increase in frequency results in an increased near field length, and thus it could be the cause. It is unclear whether this is an effect that only appears in a

	Transducer 1		Transducer 2	
	CR_{benign}	$CR_{malignant}$	CR_{benign}	$CR_{malignant}$
0 mm	0.0662	0.3845	0.2201	0.4223
1 mm	0.0986	0.3641	0.1623	0.4204
2 mm	0.1002	0.3814	0.1873	0.4779
3 mm	0.2063	0.4614	0.2662	0.3960

Table 4.3: Mass contrast ratio for each density level (extremely dense breast)

	Transducer 1		Transducer 2	
	CR_{benign}	$CR_{malignant}$	CR_{benign}	$CR_{malignant}$
0 mm	0.0229	0.3401	0.2685	0.3878
1 mm	0.1984	0.4065	0.2102	0.4486
2 mm	0.1804	0.4407	0.2147	0.3748
3 mm	0.1622	0.3420	0.2669	0.4583
7 mm	0.1235	0.2723	0.1579	0.3611

Table 4.4: Mass contrast ratio for different distances (heterogeneously dense breast)

simulated environment or if it does so in a real setup as well. One possible solution to this is to implement different gain values for the near field and the far field.

Computing for the contrast ratio values, there seems to be a decreasing trend as the frequency goes up, for both the cases of benign and malignant masses, as seen in Table A.1 in Appendix A.1. To see whether this persists in other breast density level, the same set of experiments were executed with the fatty breast specimen. While processing the results of the fatty breast experiments, it was found that the gain values had to be readjusted. As also shown in the Table A.1, the decreasing trend is also visible with the fatty breast specimen. As discussed in Chapter 2, higher frequency results in a better contrast resolution, which is important for differentiation of solid masses within structure. That in our results the contrast ratio decreases with higher frequency is interesting, because by using contrast ratio as a metric describing the ability of the system to distinguish the mass presence, it seems that higher frequency leads to poorer performance. This is most likely due to the high peak that is visible at the beginning of the output. Therefore, the solution of separating the gain values for the near field and the far field is implemented. The resulting outputs are displayed in Figure A.1 in Appendix A.1.

The results of the recalculation of the contrast ratio is shown in 4.5. The values are now more in line with the theory, where an increase in frequency creates a higher contrast, for the most part. The use of separate gain values for the near field and the far field is therefore important for higher frequencies. It is also seen that the contrast ratio values yielded are greater for the higher frequency in the case of a malignant mass, while the values are roughly the same for a benign mass. This aligns with what was discussed in Section 4.1.3, where it was mentioned that this is most likely caused by the spicules on the mass, as well as the speed of sound of malignant mass, compared to benign mass.

The maximum frequency that the toolbox is able to run depends largely on the size of the computation grid. In our case, where the computation grid is of size $500 \times 300 \times 300$, the maximum allowed frequency is 7.1 MHz.

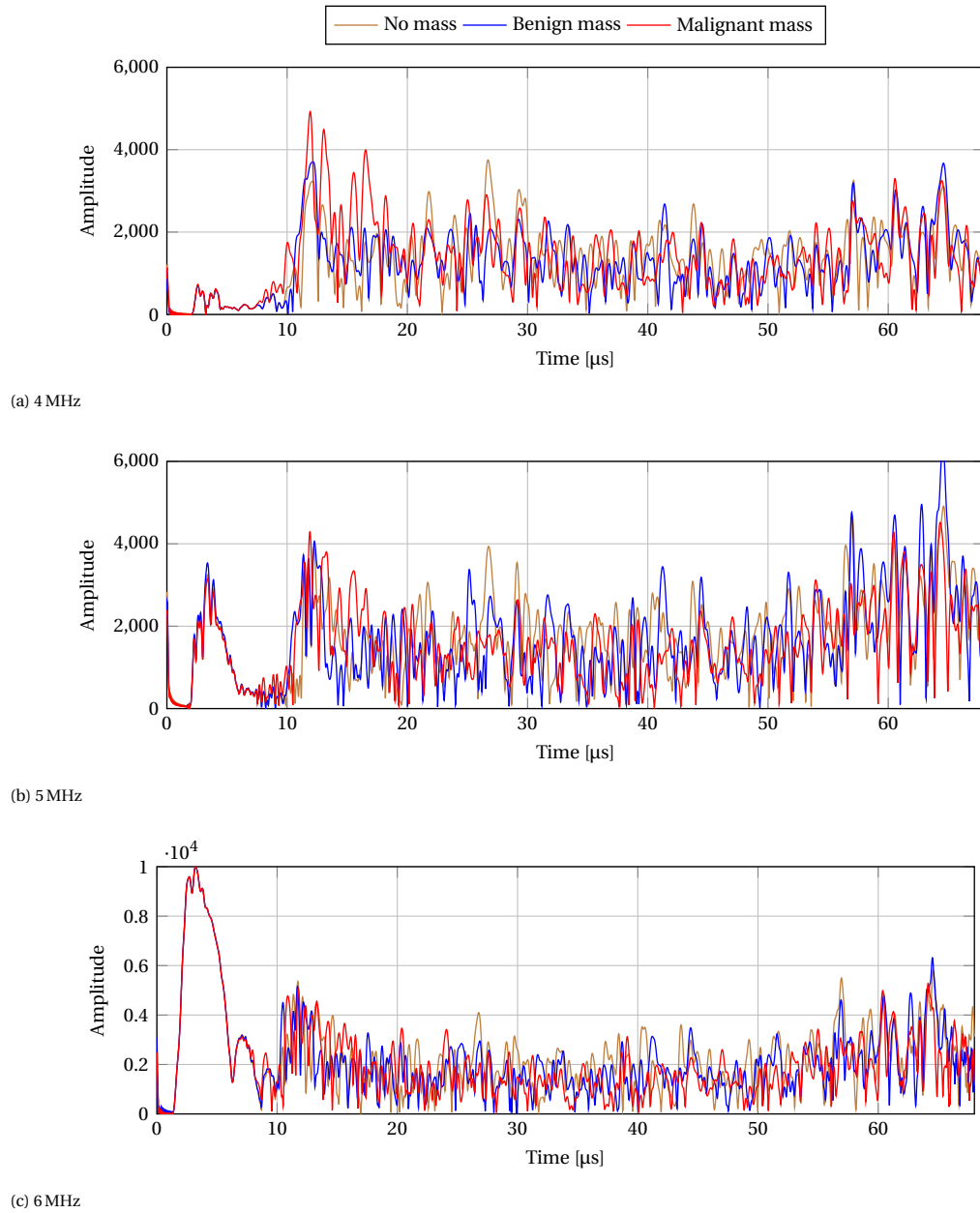


Figure 4.5: Time-domain echo response for different center frequencies of the input signal

	Heterogeneous		Fatty	
	CR_{benign}	$CR_{malignant}$	CR_{benign}	$CR_{malignant}$
3.5 MHz	0.2695	0.5024	0.3077	0.4261
4.0 MHz	0.3761	0.5379	0.2438	0.4018
4.5 MHz	0.2802	0.5123	0.2511	0.4307
5.0 MHz	0.2890	0.5201	0.2580	0.4330
6.0 MHz	0.3806	0.5701	0.1261	0.3583

Table 4.5: Mass contrast ratio for each density level

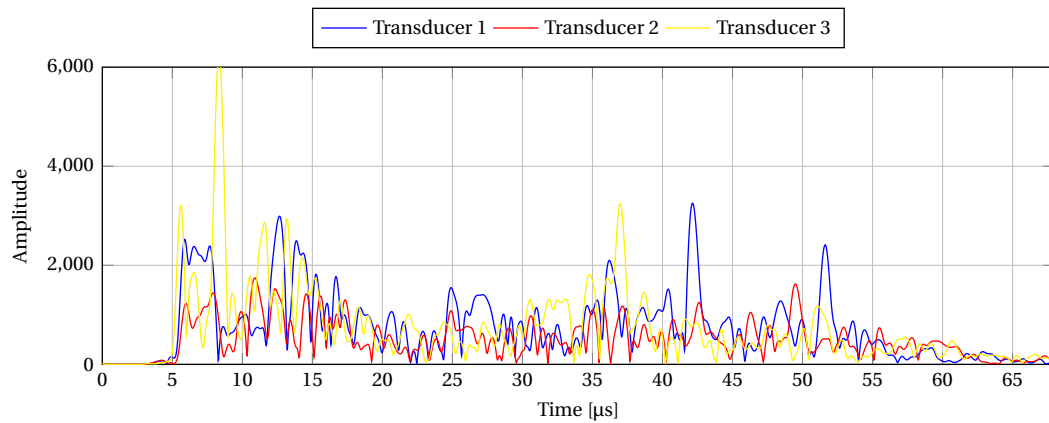


Figure 4.6: 3 transducers spaced at 2 mm for a dense breast with a malignant mass

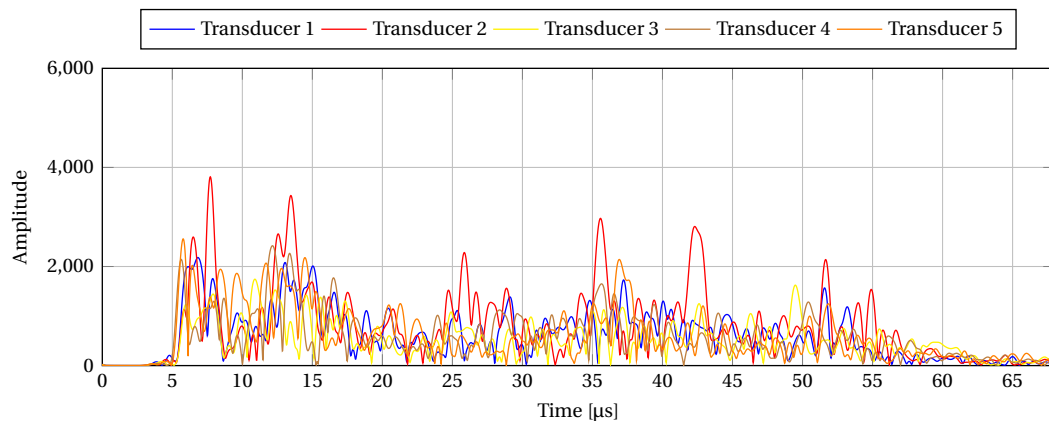


Figure 4.7: 5 transducers spaced at 1 mm for a dense breast with a malignant mass

4.4. Number of Transducers

Naturally, a higher number of transducers will result in a greater chance of having at least one of them transmit an ultrasound pulse that would hit the abnormal mass. For example, when the probe has 3 transducers that are 2 mm apart from one another, we obtain the response shown in Figure 4.6 (dense breast, malignant mass). We observe that there is high peak in the response of the third transducer, possibly because the ultrasound pulse encountered a highly spiculated area on the mass, which resulted in a strong deflection.

This parameter is closely tied with the distance parameter. The configuration of 3 transducers with a distance of 2 mm is equal in width with a configuration of 5 transducers with a distance of 1 mm. The response, however, as shown in Figure 4.7, is not exactly similar. The strongest peak is observed in the response of transducer 2, although the amplitude is not as high as that of the highest peak of the previous response.

Now we reduce the number of transducers from 5 to 4, while maintaining the distance. The results are shown in Figure 4.8. Interestingly, quite similar to the first configuration, we can see that there is a very large peak in the response of the last (right-most) transducer. Due to the large simulation time needed, especially with multiple transducers, this parameter is not tested with other breast density levels.

4.5. Comparison with B-mode

The effect of speckles that are obvious in B-mode images are also visible in the results that we obtained. Speckles are the grainy characteristic of B-mode images, where the pixels in the images have a sparse distribution of various levels of gray. Since B-mode images are essentially built upon a collection of A-lines, in terms of amplitude, speckles can be attributed as the many peaks and troughs echo lines, which is visible in

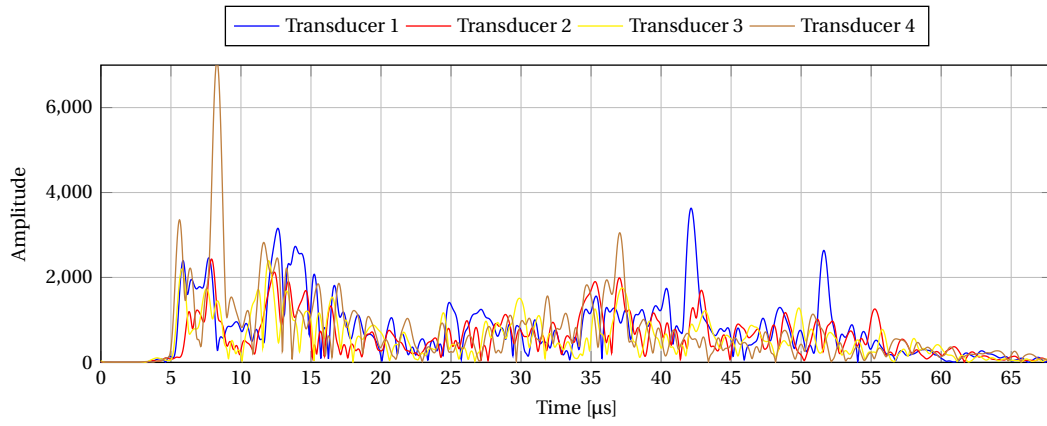


Figure 4.8: 4 transducers spaced at 2 mm for a dense breast with a malignant mass

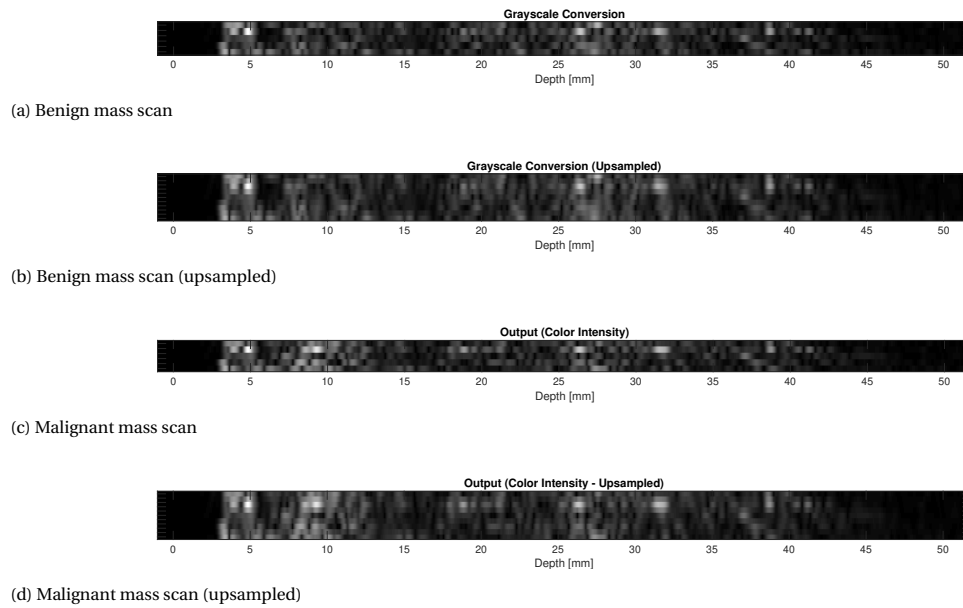


Figure 4.9: Results of grayscale conversion for simulation with 5 transducers, spaced 1 mm apart (extremely dense breast)

all the results as shown in this chapter.

In attempt to make a more thorough comparison with B-mode imaging, we take the results of a simulation with 5 transducers, placed 1 mm apart from each other, and convert them into grayscale lines shown in Figure 4.9. The image has 5 rows of pixels, corresponding to each transducer. The x-axis has been transformed from time to depth by creating a radius variable, following examples in the k-Wave documentation, using Equation 4.1, where c_0 is the reference speed of sound, t is time, dt is the discrete time difference of the response ($\frac{1}{F}$, with frequency F of the input signal), and t_0 is the middle of the input signal, time-wise.

$$r = c_0 \left(t \cdot \frac{dt}{2} - t_0 \right) \quad (4.1)$$

Upon visual inspection of Figure 4.9a, a scan result on extremely dense breast with a benign mass, there is a hint of a distinct, mass-like structure at a location close to the surface. The shape cannot be identified, however, it is an area that is rather uniformly darker than the other areas. In a traditional B-scan of a benign mass within breast tissue, the mass typically appears as a dark circle in the image, with circumscribed margins. While our result does not have that exact look, the dark, mass-like shape does bear a slight resemblance.

We note that there is a space of 1 mm between the transducers. In order to account for this space, a 2D

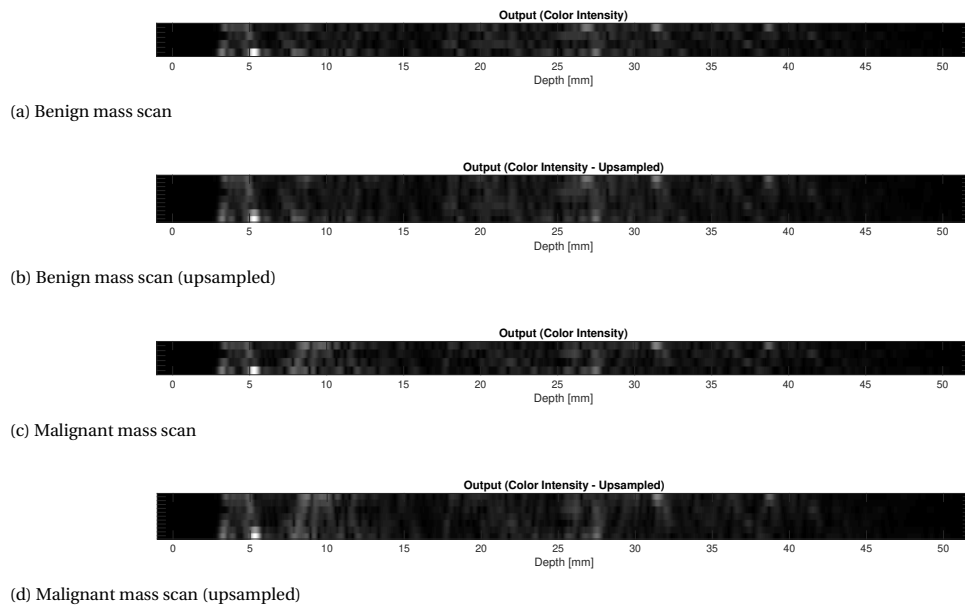


Figure 4.10: Results of grayscale conversion for simulation with 4 transducers, spaced 2 mm apart (extremely dense breast)

interpolation function is implemented on the image, using the `interp2` function on MATLAB. The resulting image is shown in Figure 4.9b. The mass-like structure is now more visible than in the original image, although the shape is still arbitrary, and the margins are not as firm as it would normally appear in a B-mode image.

When the same process above is applied to the scan output of the extremely dense breast with a malignant mass, the resulting images are displayed in Figures 4.9c and 4.9d. Looking at the two figures, contrary to the images of the benign scan, there does not seem to be any distinguishable structure where the mass should be in the malignant scan. This may be related to the ultrasonographic properties of a malignant mass. In a traditional B-scan of a malignant mass, the mass would normally have an irregular shape and spiculated margins. Since the output of our system contains a lot less information than that of a B-scan system, the resulting image is not able to correctly show a distinguishable malignant structure due to insufficiency of information.

The appearance of the mass-like structure does not always appear. When only four transducers are used, there only seems to be a patch of blackness near the skin surface, as seen in Figure 4.10. This is the case with both the benign (Figure 4.10a and 4.10b) and malignant mass (Figure 4.10c and 4.10d), albeit the patch is more visible with the malignant mass. This may indicate that a higher number of transducers may ultimately lead to better identification of a mass presence, as the system is able to contain more information.

In terms of acoustic shadowing, it seems that the effect is not discernible in either of the results for the malignant mass scan. Acoustic artifacts are the dark region (shadow) that appears behind a malignant mass. With B-mode images, this artifact is a lot easier to spot since they would be a lot darker than other structure in the lateral dimension. Since the output of our system only has a small number of scan lines (corresponding to the number of transducers), converting it into a grayscale results in a narrow image, even after upsampling the image.

4.6. Transducer Size

Besides the three parameters that were varied in order to examine the optimal values, there are many other parameters that remained constant for all the experiments. One of them is the size of the transducer, where the width is 1.3λ , and the length is 0.8 mm. An experiment is ran with a size that is four times the original size: 2.6 λ by 1.6 mm, with an input frequency of 3 MHz ($\lambda = \frac{c_0}{F} = 5.133 \times 10^{-4}$) for a heterogeneously dense breast. The results are shown in Table 4.6. It can be observed from this table that the larger transducer performs

	CR_{benign}	$CR_{malignant}$
0.7×0.8 mm	0.1433	0.3670
1.3×1.6 mm	0.2213	0.3822

Table 4.6: Different transducer size

slightly better in terms of the contrast ratio on the masses. However, there would be trade-off between the size of the transducer and the number of transducer used. In the end, the ultrasound device cannot be too large, since it only needs to cover a small area on the breast. When the transducer size is too large, only a smaller number of transducers can be used.

4.7. Comparison with Real Data

While it would be interesting to compare the scan results obtained from the simulation with real data recorded from an actual ultrasound probe, unfortunately, such data is not available in literature. Most available ultrasound datasets are in the form of grayscale images. One dataset that contain raw A-scans is publicly available. However, the data was acquired from scans of calf muscles, and therefore cannot be directly compared with our results.

5

Conclusion

The objective of this thesis is to investigate the design parameters for the development of an ultrasound device that uses several single-element (A-mode) transducers, to be used for the purpose of breast imaging. To this end, a simulation environment was built on MATLAB and C++ that uses the k-Wave toolbox and digital breast models generated from software in the Virtual Imaging Clinical Trial for Regulatory Evaluation (VICTRE) trial. The breast models are 3D volume, with each voxel assigned a tissue type. In the simulation environment, they were associated with the corresponding acoustic parameters, namely speed of sound and density, whose values were taken from literature. In relation to **RQ2**, with regards to design requirements, four different breast models with varying degrees of density were used, to test whether a certain parameter could perform as well as it does in different density level.

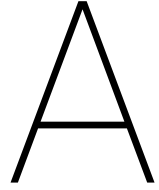
To answer **RQ1**, the design parameters that were investigated were as follows: distance between the transducers, input frequency, and number of transducers. The output of a simulation run is compared with one another using contrast ratio as a metric. Contrast ratio is the average gray-scale level of brightness (the amplitude in the case of A-scans) in the object compared to the surrounding tissue. A higher value is better as it indicates a better contrast. For the parameter distance between transducers, 3 mm yielded the best performance, although there was no linear correlation between the distance between transducers and the resulting contrast ratio. However, naturally, the results are poor when the distance are larger than the size of the mass. For input frequency, the performance increases as the frequency becomes higher, as supported by the theory. It was found in the experiments that for higher frequencies, the near field requires an implementation of different gain value than the far field. For the parameter distance between transducers, in terms of contrast ratio, it was deduced that there was no correlation between the parameter and the contrast ratio. However, in attempt to answer **RQ2** by comparing the results to artifacts in A-mode, the results of the multiple transducers were converted into grayscale. It was found there that there was a slight resemblance to a mass-like structure in the resulting narrow image. This was clearer when the image was upsampled using a 2D interpolation. The converted image also showed a better resemblance of the mass with more transducers used, even though it was still difficult in the case of a malignant mass. Ultrasonographic properties that typically appear in B-mode images, such as posterior acoustic shadowing and rigid margins in benign mass, were not discernible in the results. The parameters distance between transducers and the number of transducers are related to one another. Given a fixed size, a smaller distance would allow for more transducers to be placed. Although, in our experiments, higher distance values seemed to provide superior performance (albeit it must be smaller than the mass size). In general, the system yielded a higher contrast ratio value with malignant mass, compared to benign mass.

This thesis study had several limitations. The main one is the curbed number of experiments, as each experiment requires up to 7.5 hours per transducer, to complete. For each parameter value that is being tested, three simulations are carried out, one for when there is no mass within the breast model, one for when a benign mass is present, and one for when a malignant mass is present. Additionally, except for the comparison with B-mode images, the output of the system was mostly compared using only one metric. The simulation also only assumed one position for the probe (at the center, directly parallel from the mass). As

demonstrated during the analysis of transducer distance, even the slightest change in position resulted in a huge difference in the results. In the real world, there is very high chance that the user would not place the device directly facing the mass. Lastly, only one depth value of the mass was investigated. The mass was located around 8 mm from the skin surface.

For future work, a study with results from a physical A-mode device could be carried out. This study only relied on results of a simulation and in the real world, there are often circumstances that would make the output a lot different, such as noise or the positioning of the transducer, as it would be handheld by a person and not statistically placed like in the simulations. This study focused on the optimization of the design parameters of the ultrasound device, and as mentioned early on, the next step would be to design an algorithm that is able to identify the presence of the mass and determine its malignancy using the A-scan output of the system. Different signal processing methods may also be explored as there are recent, novel methods used in B-mode imaging. It would be interesting to see whether the methods are applicable in our proposed system. The development of this device is still a long way to go, as it would also need to undergo clinical study before it could be used by the public.

In the end, this thesis study acts as a first step towards the development of an affordable, ultrasound device that women could use for breast scanning, from the comfort of their home. Ultimately, this study should be treated as a precursor to more research in the use of multiple A-mode transducers for breast imaging. While it was not generally mentioned throughout this report, the design parameters are also closely tied to the costs of manufacturing the device, which is an important constraint considering the aim to make it affordable. Other factors such as the size or dimension of the device are also related to the parameters and as such, would need to be considered in further development of the device.



Complementary Results

A.1. Various Input Frequencies

	Heterogeneous		Fatty	
	CR_{benign}	$CR_{malignant}$	CR_{benign}	$CR_{malignant}$
3.5 MHz	0.1433	0.3670	0.3678	0.4882
4.0 MHz	0.2213	0.3822	0.4401	0.5412
4.5 MHz	0.0993	0.3201	0.2335	0.4117
5.0 MHz	0.0483	0.2722	0.3199	0.4759
6.0 MHz	0.0284	0.0304	0.1456	0.3087

Table A.1: Mass contrast ratio for each density level

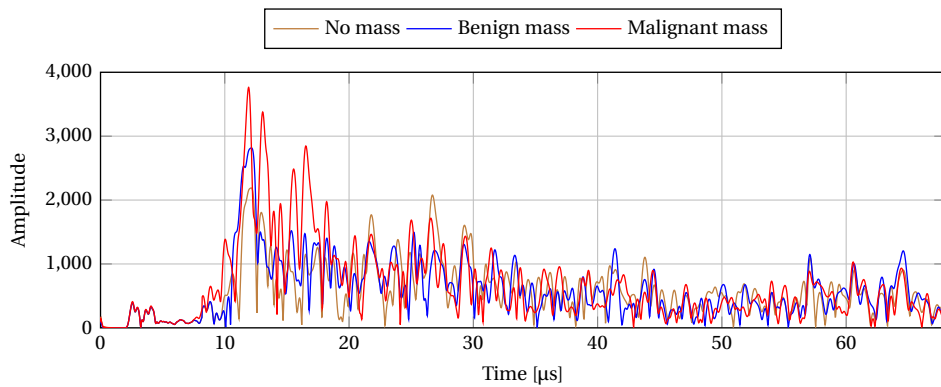
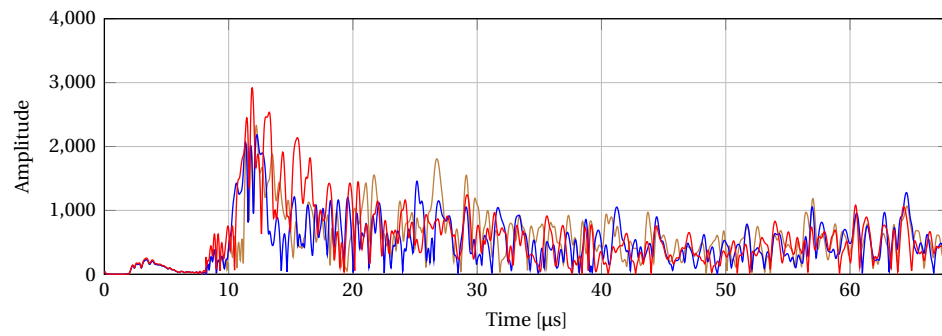
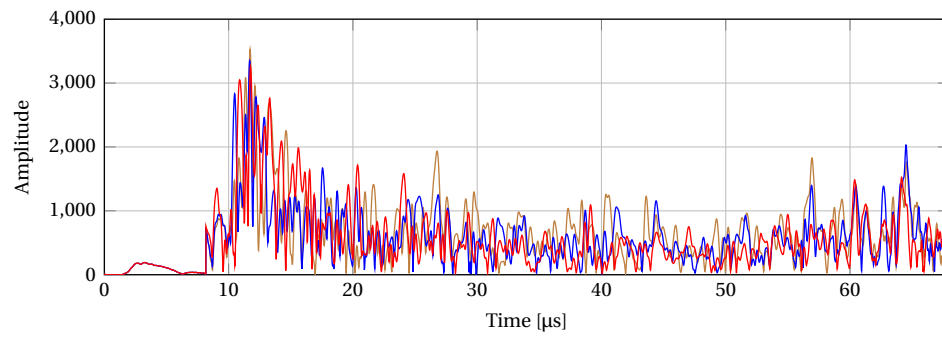


Figure A.1: Time-domain echo response for different center frequencies of the input signal



(b) 5 MHz



(c) 6 MHz

Figure A.1: Time-domain echo response for different center frequencies of the input signal

A.2. Various Transducer Distance

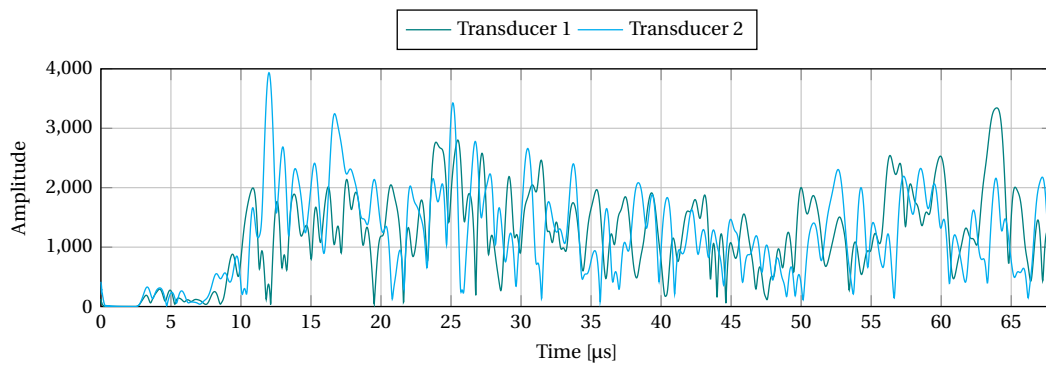


Figure A.2: Two transducers placed next to each other (heterogeneously dense breast with a benign mass at 3 MHz).

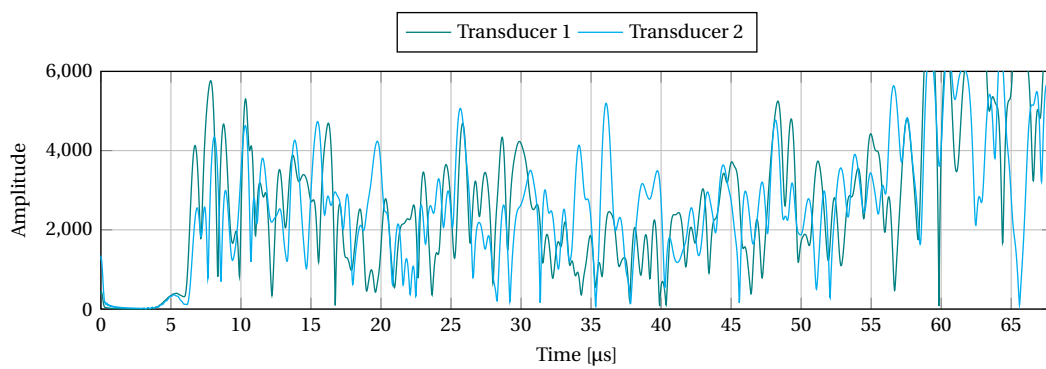


Figure A.3: Two transducers placed next to each other (scattered density breast with a benign mass at 3 MHz).

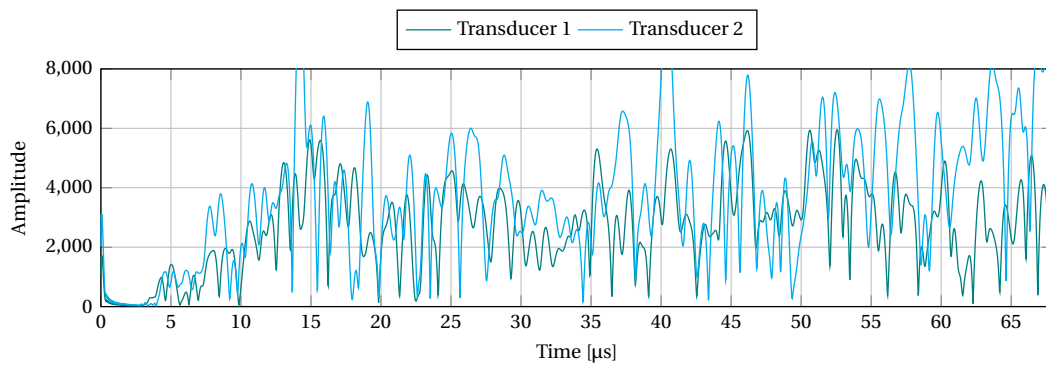


Figure A.4: Two transducers placed next to each other (fatty breast with a benign mass at 3 MHz).

Bibliography

- [1] F. Bray, J. Ferlay, I. Soerjomataram, R. L. Siegel, L. A. Torre, and A. Jemal. Global cancer statistics 2018: Globocan estimates of incidence and mortality worldwide for 36 cancers in 185 countries. *CA: A Cancer Journal for Clinicians*, 68(6):394–424, 2018. doi: 10.3322/caac.21492. URL <https://acsjournals.onlinelibrary.wiley.com/doi/abs/10.3322/caac.21492>.
- [2] R. L. Siegel, K. D. Miller, S. A. Fedewa, D. J. Ahnen, R. G. S. Meester, A. Barzi, and A. Jemal. Colorectal cancer statistics, 2017. *CA: A Cancer Journal for Clinicians*, 67(3):177–193, 2017. ISSN 0007-9235. doi: 10.3322/caac.21395. URL <https://doi.org/10.3322/caac.21395>.
- [3] K. C. Oeffinger, E. T. H. Fontham, R. Etzioni, A. Herzig, J. S. Michaelson, Y.-C. T. Shih, L. C. Walter, T. R. Church, C. R. Flowers, S. J. LaMonte, A. M. D. Wolf, C. DeSantis, J. Lortet-Tieulent, K. Andrews, D. Manassaram-Baptiste, D. Saslow, R. A. Smith, O. W. Brawley, and R. Wender. Breast Cancer Screening for Women at Average Risk: 2015 Guideline Update From the American Cancer Society. *JAMA*, 314(15):1599–1614, 10 2015. ISSN 0098-7484. doi: 10.1001/jama.2015.12783. URL <https://doi.org/10.1001/jama.2015.12783>.
- [4] American Cancer Society. *Cancer Facts & Figures 2020*. American Cancer Society, Atlanta, GA, 2020.
- [5] A. Sencha, E. Evseeva, M. Mogutov, and Y. Patrunov. *Breast Ultrasound*. Springer, Berlin, Heidelberg, 03 2013. ISBN 978-3-642-36501-0. doi: 10.1007/978-3-642-36502-7_7.
- [6] R. Ferrini, E. Mannino, E. Ramsdell, and L. Hill. Screening mammography for breast cancer: American college of preventive medicine practice policy statement. *American Journal of Preventive Medicine*, 12(5):340 – 341, 1996. ISSN 0749-3797. doi: [https://doi.org/10.1016/S0749-3797\(18\)30289-7](https://doi.org/10.1016/S0749-3797(18)30289-7). URL <http://www.sciencedirect.com/science/article/pii/S0749379718302897>. Women’s Health in the 1990s.
- [7] M. J. Anderson and P. J. Whitcomb. *Design of Experiments*, pages 1–22. American Cancer Society, 2010. ISBN 978-0-471-23896-6. doi: 10.1002/0471238961.0405190908010814.a01.pub3. URL <https://onlinelibrary.wiley.com/doi/abs/10.1002/0471238961.0405190908010814.a01.pub3>.
- [8] X. Xu, C. Gifford-Hollingsworth, R. Sensenig, W.-H. Shih, W. Y. Shih, and A. D. Brooks. Breast tumor detection using piezoelectric fingers: First clinical report. *Journal of the American College of Surgeons*, 216(6):1168 – 1173, 2013. ISSN 1072-7515. doi: <https://doi.org/10.1016/j.jamcollsurg.2013.02.022>. URL <http://www.sciencedirect.com/science/article/pii/S1072751513001683>.
- [9] R. B. Broach, R. Geha, B. S. Englander, L. DeLaCruz, H. Thrash, and A. D. Brooks. A cost-effective handheld breast scanner for use in low-resource environments: a validation study. *World Journal of Surgical Oncology*, 14(1):277, Oct 2016. ISSN 1477-7819. doi: 10.1186/s12957-016-1022-2. URL <https://doi.org/10.1186/s12957-016-1022-2>.
- [10] S. P. Somashekhar, R. Vijay, R. Ananthasivan, and G. Prasanna. Noninvasive and low-cost technique for early detection of clinically relevant breast lesions using a handheld point-of-care medical device (ibreastexam): Prospective three-arm triple-blinded comparative study. *Indian Journal of Gynecologic Oncology*, 14(2):26, Apr 2016. ISSN 2363-8400. doi: 10.1007/s40944-016-0057-1. URL <https://doi.org/10.1007/s40944-016-0057-1>.
- [11] S. Nair, T. Kathrikolly, and P. P. Saxena. Abstract p1-01-01: Clinical efficacy evaluation of a novel palpation imaging device for early detection of breast cancer in the developing world. *Cancer Research*, 80(4 Supplement):P1-01-01–P1-01-01, 2020. ISSN 0008-5472. doi: 10.1158/1538-7445.SABCS19-P1-01-01. URL https://cancerres.aacrjournals.org/content/80/4_Supplement/P1-01-01.

- [12] M. Haas. Business for good: ibreastexam. *The Philadelphia Citizen*, May 2019. URL <https://thephiladelphiacitizen.org/business-for-good-ibreastexam/>. Retrieved on 28-08-2020.
- [13] S. M. Love, W. A. Berg, C. Podilchuk, A. L. López Aldrete, A. P. Gaxiola Mascareño, K. Pathicherikollamparambil, A. Sankarasubramanian, L. Eshraghi, and R. Mammone. Palpable breast lump triage by minimally trained operators in mexico using computer-assisted diagnosis and low-cost ultrasound. *Journal of Global Oncology*, (4):1–9, 2018. doi: 10.1200/JGO.17.00222. URL <https://doi.org/10.1200/JGO.17.00222>. PMID: 30156946.
- [14] General Electric Company. Vscan extend r2 with dual probe. *GE Healthcare US Store*, 2020. URL <https://store.gehealthcare.com/en-us/products/point-of-care/vscan-extend-r2-dual-probe>. Retrieved on 28-08-2020.
- [15] A. E. Smith-Ryan, S. N. Fultz, M. N. Melvin, H. L. Wingfield, and M. N. Woessner. Reproducibility and validity of a-mode ultrasound for body composition measurement and classification in overweight and obese men and women. *PLOS ONE*, 9(3):1–8, 03 2014. doi: 10.1371/journal.pone.0091750. URL <https://doi.org/10.1371/journal.pone.0091750>.
- [16] BodyMetrix. Bodymetrix professional. *BodyMetrix Shop*, 2020. URL <https://shop.intelamatrix.com/shop?olsPage=products%2Fbodymetrix-professional>. Retrieved on 28-08-2020.
- [17] D. R. Wagner, M. Teramoto, T. Judd, J. Gordon, C. McPherson, and A. Robison. Comparison of a-mode and b-mode ultrasound for measurement of subcutaneous fat. *Ultrasound in Medicine & Biology*, 46(4):944 – 951, 2020. ISSN 0301-5629. doi: <https://doi.org/10.1016/j.ultrasmedbio.2019.11.018>. URL <http://www.sciencedirect.com/science/article/pii/S030156291931600X>.
- [18] J. Wild and D. Neal. Use of high-frequency ultrasonic waves for detecting changes of texture in living tissues. *The Lancet*, 257(6656):655 – 657, 1951. ISSN 0140-6736. doi: [https://doi.org/10.1016/S0140-6736\(51\)92403-8](https://doi.org/10.1016/S0140-6736(51)92403-8). URL <http://www.sciencedirect.com/science/article/pii/S0140673651924038>. Originally published as Volume 1, Issue 6656.
- [19] G. D. Ludwig. The velocity of sound through tissues and the acoustic impedance of tissues. *The Journal of the Acoustical Society of America*, 22(6):862–866, 1950. doi: 10.1121/1.1906706. URL <https://doi.org/10.1121/1.1906706>.
- [20] N. J. Hangiandreou. AAPM/RSNA physics tutorial for residents: Topics in US. *RadioGraphics*, 23(4):1019–1033, July 2003. doi: 10.1148/rg.234035034. URL <https://doi.org/10.1148/rg.234035034>.
- [21] S. P. Weinstein, E. F. Conant, and C. Sehgal. Technical advances in breast ultrasound imaging. *Seminars in Ultrasound, CT and MRI*, 27(4):273 – 283, 2006. ISSN 0887-2171. doi: <https://doi.org/10.1053/j.sult.2006.05.002>. URL <http://www.sciencedirect.com/science/article/pii/S0887217106000436>. Breast Imaging Update.
- [22] A. Athanasiou, A. Tardivon, L. Ollivier, F. Thibault, C. E. Khoury, and S. Neuenschwander. How to optimize breast ultrasound. *European Journal of Radiology*, 69(1):6 – 13, 2009. ISSN 0720-048X. doi: <https://doi.org/10.1016/j.ejrad.2008.07.034>. URL <http://www.sciencedirect.com/science/article/pii/S0720048X08004488>. Breast Imaging.
- [23] M. Mahesh. The essential physics of medical imaging, third edition. *Medical Physics*, 40(7):077301, 2013. doi: 10.1118/1.4811156. URL <https://aapm.onlinelibrary.wiley.com/doi/abs/10.1118/1.4811156>.
- [24] T. Whittingham and K. Martin. Transducers and beam-forming. In P. R. Hoskins, K. Martin, and A. Thrush, editors, *Diagnostic Ultrasound: Physics and Equipment*, chapter 3. Cambridge University Press, 2 edition, 2010. ISBN 978-0-521-75710-2. doi: 10.1017/CBO9780511750885.
- [25] T. L. Szabo. Diagnostic ultrasound imaging. Biomedical Engineering, pages 1–28, 71–96, 213–242, 535–536. Academic Press, Burlington, 2004. ISBN 978-0-12-680145-3. doi: <https://doi.org/10.1016/B978-012680145-3/50018-9>. URL <http://www.sciencedirect.com/science/article/pii/B9780126801453500189>.

- [26] B. D. Sites, R. Brull, V. W. Chan, B. C. Spence, J. Gallagher, M. L. Beach, V. R. Sites, S. Abbas, and G. S. Hartman. Artifacts and pitfall errors associated with ultrasound-guided regional anesthesia: Part ii: A pictorial approach to understanding and avoidance. *Regional Anesthesia & Pain Medicine*, 32(5):419–433, 2007. doi: 10.1016/j.rapm.2007.08.001. URL <https://rapm.bmj.com/content/32/5/419>.
- [27] S. P. Weinstein, E. F. Conant, S. G. Orel, T. J. Lawton, and G. Acs. Diabetic mastopathy in men: Imaging findings in two patients. *Radiology*, 219(3):797–799, 2001. doi: 10.1148/radiology.219.3.r01jn38797. URL <https://doi.org/10.1148/radiology.219.3.r01jn38797>. PMID: 11376272.
- [28] K. Drukker, M. L. Giger, and E. B. Mendelson. Computerized analysis of shadowing on breast ultrasound for improved lesion detection. *Medical Physics*, 30(7):1833–1842, 2003. doi: 10.1118/1.1584042. URL <https://aapm.onlinelibrary.wiley.com/doi/abs/10.1118/1.1584042>.
- [29] J. Russo, R. Rivera, and I. H. Russo. Influence of age and parity on the development of the human breast. *Breast Cancer Research and Treatment*, 23(3):211–218, October 1992. doi: 10.1007/bf01833517. URL <https://doi.org/10.1007/bf01833517>.
- [30] T. R. Milanese, L. C. Hartmann, T. A. Sellers, M. H. Frost, R. A. Vierkant, S. D. Maloney, V. S. Pankratz, A. C. Degnim, C. M. Vachon, C. A. Reynolds, R. A. Thompson, I. Melton, L. Joseph, E. L. Goode, and D. W. Visscher. Age-Related Lobular Involution and Risk of Breast Cancer. *JNCI: Journal of the National Cancer Institute*, 98(22):1600–1607, 11 2006. ISSN 0027-8874. doi: 10.1093/jnci/djj439. URL <https://doi.org/10.1093/jnci/djj439>.
- [31] Johns Hopkins University. Overview of the breast: Breast pathology. *Johns Hopkins University*, 2020. URL <https://pathology.jhu.edu/breast/overview/>.
- [32] J. Russo, Y.-F. Hu, X. Yang, and I. H. Russo. Chapter 1: Developmental, Cellular, and Molecular Basis of Human Breast Cancer. *JNCI Monographs*, 2000(27):17–37, 07 2000. ISSN 1052-6773. doi: 10.1093/oxfordjournals.jncimonographs.a024241. URL <https://doi.org/10.1093/oxfordjournals.jncimonographs.a024241>.
- [33] G. Rahbar, A. C. Sie, G. C. Hansen, J. S. Prince, M. L. Melany, H. E. Reynolds, V. P. Jackson, J. W. Sayre, and L. W. Bassett. Benign versus malignant solid breast masses: Us differentiation. *Radiology*, 213(3):889–894, 1999. doi: 10.1148/radiology.213.3.r99dc20889. URL <https://doi.org/10.1148/radiology.213.3.r99dc20889>. PMID: 10580971.
- [34] J. J. James and A. J. Evans. Breast. In P. L. Allan, G. M. Baxter, and M. J. Weston, editors, *Clinical Ultrasound*, chapter 49, pages 987–1004. Churchill Livingstone Elsevier, 3 edition, 2011. ISBN 978-0-702-05024-4.
- [35] S. P. Weinstein, E. F. Conant, C. Mies, G. Acs, S. Lee, and C. Sehgal. Posterior acoustic shadowing in benign breast lesions. *Journal of Ultrasound in Medicine*, 23(1):73–83, 2004. doi: 10.7863/jum.2004.23.1.73. URL <https://onlinelibrary.wiley.com/doi/abs/10.7863/jum.2004.23.1.73>.
- [36] American College of Radiology. Acr bi-rads®-mammography: Breast imaging reporting and data system. *Breast Imaging Atlas*, 2003.
- [37] R. A. Smith and C. J. D’Orsi. Screening for breast cancer. In J. R. Harris, M. E. Lippman, M. Morrow, and C. K. Osborne, editors, *Diseases of the Breast*, chapter 11. Lippincott Williams & Wilkins, 2 edition, 2000. ISBN 978-0-781-71839-4.
- [38] J. M. H. Timmers, H. J. van Doorne-Nagtegaal, H. M. Zonderland, H. van Tinteren, O. Visser, A. L. M. Verbeek, G. J. den Heeten, and M. J. M. Broeders. The breast imaging reporting and data system (bi-rads) in the dutch breast cancer screening programme: its role as an assessment and stratification tool. *European Radiology*, 22(8):1717–1723, Aug 2012. ISSN 1432-1084. doi: 10.1007/s00330-012-2409-2. URL <https://doi.org/10.1007/s00330-012-2409-2>. 22415412[pmid], PMC3387359[pmcid].
- [39] C. M. W. Daft and W. M. Leue. System and method for statistical design of ultrasound probe and imaging system, February 28 2006. URL <https://patents.google.com/patent/US20030154062>. U.S. Patent 7,006,955.

- [40] Y. Lou, W. Zhou, T. P. Matthews, C. M. Appleton, and M. A. Anastasio. Generation of anatomically realistic numerical phantoms for photoacoustic and ultrasonic breast imaging. *Journal of Biomedical Optics*, 22(4):1 – 13, 2017. doi: 10.1117/1.JBO.22.4.041015. URL <https://doi.org/10.1117/1.JBO.22.4.041015>.
- [41] A. Maidment, P. Bakic, B. Barufaldi, D. Higginbotham, D. Pokrajac, A. Avanaki, K. Espig, A. Xthona, and T. Kimpe. Openvct: A framework for open-source virtual clinical trial. *Medical Physics*, 44(6), 2017. Resources: WE-G-601-06.
- [42] B. Barufaldi, P. Bakic, D. Higginbotham, and A. Maidment. Openvct: a gpu-accelerated virtual clinical trial pipeline for mammography and digital breast tomosynthesis. page 194, 03 2018. doi: 10.1117/12.2294935. URL <https://doi.org/10.1117/12.2294935>.
- [43] A. Badano, C. G. Graff, A. Badal, D. Sharma, R. Zeng, F. W. Samuelson, S. J. Glick, and K. J. Myers. Evaluation of Digital Breast Tomosynthesis as Replacement of Full-Field Digital Mammography Using an In Silico Imaging Trial. *JAMA Network Open*, 1(7):e185474–e185474, 11 2018. ISSN 2574-3805. doi: 10.1001/jamanetworkopen.2018.5474. URL <https://doi.org/10.1001/jamanetworkopen.2018.5474>.
- [44] C. G. Graff. A new, open-source, multi-modality digital breast phantom. In D. Kontos and T. G. Flohr, editors, *Medical Imaging 2016: Physics of Medical Imaging*, volume 9783, pages 72 – 81. International Society for Optics and Photonics, SPIE, 2016. doi: 10.1117/12.2216312. URL <https://doi.org/10.1117/12.2216312>.
- [45] L. de Sisternes, J. G. Brankov, A. M. Zysk, R. A. Schmidt, R. M. Nishikawa, and M. N. Wernick. A computational model to generate simulated three-dimensional breast masses. *Medical physics*, 42(2):1098–1118, Feb 2015. ISSN 2473-4209. doi: 10.1118/1.4905232. URL <https://doi.org/10.1118/1.4905232>. 25652522[pmid], PMC4320152[pmcid].
- [46] B. T. Nicholson, A. P. LoRusso, M. Smolkin, V. E. Bovbjerg, G. R. Petroni, and J. A. Harvey. Accuracy of assigned bi-rads breast density category definitions. *Academic Radiology*, 13(9):1143 – 1149, 2006. ISSN 1076-6332. doi: <https://doi.org/10.1016/j.acra.2006.06.005>. URL <http://www.sciencedirect.com/science/article/pii/S1076633206003205>.
- [47] J. A. Jensen. Simulation of advanced ultrasound systems using field ii. In *2004 2nd IEEE International Symposium on Biomedical Imaging: Nano to Macro (IEEE Cat No. 04EX821)*, pages 636–639 Vol. 1, April 2004. doi: 10.1109/ISBI.2004.1398618. URL <https://doi.org/10.1109/ISBI.2004.1398618>.
- [48] G. E. Tupholme. Generation of acoustic pulses by baffled plane pistons. *Mathematika*, 16(2):209–224, 1969. doi: 10.1112/S0025579300008184. URL <https://londmathsoc.onlinelibrary.wiley.com/doi/abs/10.1112/S0025579300008184>.
- [49] P. R. Stepanishen. Transient radiation from pistons in an infinite planar baffle. *The Journal of the Acoustical Society of America*, 49(5B):1629–1638, 1971. doi: 10.1121/1.1912541. URL <https://doi.org/10.1121/1.1912541>.
- [50] R. J. McGough. Focus: Fast object-oriented c++ ultrasound simulator. *FOCUS | Michigan State University*, 2020. URL <https://www.egr.msu.edu/~fultras-web/>.
- [51] R. J. McGough, T. V. Samulski, and J. F. Kelly. An efficient grid sectoring method for calculations of the near-field pressure generated by a circular piston. *The Journal of the Acoustical Society of America*, 115(5 Pt 1):1942—1954, May 2004. ISSN 0001-4966. doi: 10.1121/1.1687835. URL <https://europepmc.org/articles/PMC2292796>.
- [52] R. J. McGough. Rapid calculations of time-harmonic nearfield pressures produced by rectangular pistons. *The Journal of the Acoustical Society of America*, 115(5 Pt 1):1934—1941, May 2004. ISSN 0001-4966. doi: 10.1121/1.1694991. URL <https://europepmc.org/articles/PMC2484122>.
- [53] S. Holm. Ultrasim-a toolbox for ultrasound field simulation. 01 2001.
- [54] B. E. Treeby and B. T. Cox. k-Wave: MATLAB toolbox for the simulation and reconstruction of photoacoustic wave fields. *Journal of Biomedical Optics*, 15(2):1 – 12, 2010. doi: 10.1117/1.3360308. URL <https://doi.org/10.1117/1.3360308>.

- [55] G. Taraldsen. A generalized westervelt equation for nonlinear medical ultrasound. *The Journal of the Acoustical Society of America*, 109(4):1329–1333, 2001. doi: 10.1121/1.1344157. URL <https://asa.scitation.org/doi/abs/10.1121/1.1344157>.
- [56] B. E. Treeby, J. Jaros, A. P. Rendell, and B. T. Cox. Modeling nonlinear ultrasound propagation in heterogeneous media with power law absorption using a k-space pseudospectral method. *The Journal of the Acoustical Society of America*, 131(6):4324–4336, June 2012. doi: 10.1121/1.4712021. URL <https://doi.org/10.1121/1.4712021>.
- [57] F. A. Duck. *Physical Properties of Tissues*, chapter 4, 5. Academic Press, London, 1990. ISBN 978-0-12-222800-1. doi: <https://doi.org/10.1016/B978-0-12-222800-1.50009-7>. URL <http://www.sciencedirect.com/science/article/pii/B9780122228001500097>.
- [58] B. Sohrab, G. Farzan, B. Ashkan, and J. Amin. Ultrasound thermotherapy of breast: Theoretical design of transducer and numerical simulation of procedure. *Japanese Journal of Applied Physics*, 45(3A):1856–1863, mar 2006. doi: 10.1143/jjap.45.1856. URL <https://doi.org/10.1143%2Fjjap.45.1856>.
- [59] C. Li, N. Duric, P. Littrup, and L. Huang. In vivo breast sound-speed imaging with ultrasound tomography. *Ultrasound in Medicine & Biology*, 35(10):1615 – 1628, 2009. ISSN 0301-5629. doi: <https://doi.org/10.1016/j.ultrasmedbio.2009.05.011>. URL <http://www.sciencedirect.com/science/article/pii/S0301562909002373>.